

UNIVERSIDADE DE LISBOA
FACULDADE DE CIÊNCIAS
DEPARTAMENTO DE ENGENHARIA GEOGRÁFICA, GEOFÍSICA E ENERGIA



Combining ERT, TDEM, and FDEM in Shallow Geophysical Investigation.

Pedro Alexandre Baltazar Soares

Mestrado em Ciências Geofísicas
Especialização em Geofísica Interna

Dissertação orientada por:
Prof. Dr. Fernando Acácio Monteiro Santos

Agradecimentos

A realização desta dissertação só foi possível com ajuda de determinadas pessoas às quais gostaria de deixar o meu mais profundo agradecimento.

Ao meu orientador Dr. Fernando Acácio Monteiro Santos, pela oportunidade, paciência e pelos valiosos ensinamentos transmitidos ao longo deste trabalho.

Ao Dr. Francisco Martinez Moreno, por toda ajuda que me deu, sempre pronto para ajudar e com uma disponibilidade incrível na transmissão de valiosos conhecimentos, tanto a nível de aquisição de dados, bem como teóricos. Sem dúvida que seria muito mais complicado sem a sua ajuda.

A todos os meus amigos e colegas que partilharam comigo frustrações, conquistas e desabafos, obrigado pelos aconselhamentos e paciência.

Por último, a toda a minha família por serem como são e por me acompanharem e apoiarem ao longo da vida e em especial nesta fase. Sem eles nada disto teria sido possível.

Resumo

Nesta dissertação são apresentados os resultados da combinação de três métodos geofísicos aplicados a dois casos de estudo distintos em Portugal continental, com o objetivo de comparar os resultados obtidos. Os métodos aplicados foram: Tomografia de Resistividade Elétrica (ERT), Eletromagnético no Domínio do Tempo (TDEM) e Eletromagnético no Domínio da Frequência (FDEM).

O primeiro caso de estudo localiza-se próximo a um reservatório de águas contaminadas de uma instalação industrial. O principal objetivo era detetar e definir zonas de contaminação de águas subterrâneas. Para esse efeito, foram aplicados dois métodos em dois perfis: ERT e FDEM. No primeiro perfil, o método FDEM deteta uma zona de alta resistividade na parte mais superficial (~ 25 m) e a parte superior de uma área contaminada. Os perfis de ERT atingem maiores profundidades e definem toda a área contaminada sobre uma zona não fraturada. No segundo perfil, o método FDEM deteta a parte mais superficial (~ 20 m de profundidade) com a presença de duas falhas que controlam a circulação das águas subterrâneas. Esse recurso também é detetado no perfil ERT que penetra mais profundamente, detetando a presença de duas áreas contaminadas.

O segundo caso de estudo é desenvolvido sobre uma zona aluvial próxima ao rio Tejo, onde está em construção um parque industrial. O principal objetivo é investigar se a área tem as condições necessárias para a construção do ponto de vista da engenharia. Nesta área, foram aplicados os três métodos nos três perfis: ERT, TDEM e FDEM. No primeiro perfil, a combinação dos três métodos permitiu a deteção de três camadas: uma superficial e plana com alta resistividade (origem antrópica), sobre uma área de resistividade muito baixa, com morfologia heterogénea (sedimentos com grande quantidade de argilas) e, no fundo, uma área de resistividade intermediária (rocha e águas subterrâneas). O segundo perfil foi adquirido paralelamente ao primeiro e combina as técnicas ERT e TDEM. Ambos detetaram as mesmas camadas do primeiro perfil, com formas diferentes, o leito rochoso é mais superficial e mergulha em direção a noroeste. O terceiro perfil estava localizado perpendicularmente aos anteriores. Este perfil (ERT) deteta e define as falhas na zona de estudo.

Além disso, foi realizado o cálculo da resistividade aparente e posterior inversão para os dados do FDEM-8. Os resultados são muito encorajadores, em que na maioria dos perfis foi obtida uma resposta quantitativa de acordo com os outros métodos utilizados (ERT e TDEM). No entanto, é necessário mais trabalho para obter um melhor modelo otimizado que permita uma interpretação detalhada.

Esta investigação demonstra a complementaridade dos métodos geofísicos utilizados. O método ERT deteta os recursos no subsolo com mais detalhes. O TDEM e o FDEM definem melhor a localização das camadas condutoras, pois são muito sensíveis à presença de material condutor. Os três métodos são muito apropriados para serem aplicados em casos semelhantes de estudo, tanto em hidrogeologia quanto em engenharia.

PALAVRAS-CHAVE: Tomografia Eléctrica de Resistividade (ERT), Electromagnético no Dominio do Tempo (TDEM), Electromagnético no Dominio da Frequência (FDEM), Engenharia Geotécnica e Ambiental, Inversão dos dados FDEM-8.

Abstract

The combination of three geophysical methods in two different case studies is presented in this dissertation. The applied methods were Electrical Resistivity Tomography (ERT), Time-Domain Electromagnetic (TDEM) and Frequency-Domain Electromagnetic (FDEM). Two different areas in Portugal (onshore) were selected aimed to compare the results obtained in the different methods.

The first case study is located close to the contaminated water reservoir of an industrial facility. The main objective in this area was to detect and define the contamination zones and features that constrain the groundwater circulation. Here, two methods were applied along two profiles: ERT and FDEM. At the first profile, FDEM methods detect a high resistivity zone at the shallower part (~25 m) and the upper part of a contaminated area. ERT goes deeper depths and defines the whole contaminated area over a non-fractured zone. At the second profile, the FDEM method detects the shallower part (~20 m depth) with the presence of two faults that control the groundwater circulation. This feature is also detected in the ERT profile that penetrates deeper, detecting the presence of two contaminated areas.

The second case of study is developed over an alluvial zone close to the Tajo River where an industrial park is under construction. The main objective is to investigate if the area is appropriate for construction from an engineering point of view. In this area, three methods along 3 profiles were applied: ERT, TDEM, and FDEM. In the first profile the combination of the three methods allowed the detection of 3 layers: a flat shallower area with high resistivity (anthropic origin), over a very low resistivity area with heterogeneous morphology (sediment with high quantity of clays) and, at the bottom, an intermediate resistivity area (bedrock and groundwater). The second profile was acquired parallel to the first and it combines ERT and TDEM techniques. Both detected the same layers as in the first profile with different shapes, the bedrock is shallower and that dipping toward NW. The third profile was located perpendicular to the previous ones. This profile (ERT) detects and defines the faults in the area.

Additionally, an optimization of the apparent resistivity calculation and further inversion for FDEM-8 data were performed. The results are very encouraging, wherein most profiles a quantitative response was obtained in agreement with the other methods (ERT and TDEM). However, more work is needed in order to obtain a better method that allows detailed interpretation.

This investigation demonstrates the complementarity of the used geophysical methods. ERT method detects the features at the subsoil with more detail. TDEM defines better the location of the conductive layers since it is very sensitive to the presence of conductive material such as FDEM. The three methods are very appropriate to be applied in similar cases of study, both, hydrogeology and engineering purposes.

KEY WORDS: Electrical resistivity tomography (ERT), Time-Domain Electromagnetic (TDEM), Frequency-Domain Electromagnetic (FDEM), Geotechnical and Environmental Engineering, FDEM-8 data inversion.

Contents

AGRADECIMENTOS.....	I
RESUMO.....	II
ABSTRACT.....	V
CONTENTS.....	VII
I. LIST OF FIGURES.....	IX
II. LIST OF TABLES.....	XI
1. COMBINING ERT, TDEM, AND FDEM IN SHALLOW GEOPHYSICAL INVESTIGATION.....	1
1.1. INTRODUCTION.....	1
1.1.1. Thesis Framework.....	1
1.1.2. History and state-of-art of Applied Geophysics.....	2
1.2. PROPERTIES OF NEAR-SURFACE SOILS.....	4
1.2.1. Electric Properties.....	4
1.2.2. Electromagnetic properties.....	6
1.2.3. Electronic, Semi-Conductive and Electrolyte Conduction.....	7
1.2.3.1. Electronic Conduction.....	7
1.2.3.2. Semi-conductive Conduction.....	8
1.2.3.3. Electrolytic Conduction.....	8
1.2.4. Effects on Electrolyte Conduction.....	9
1.2.4.1. Effect of Temperature.....	9
1.2.4.2. Effect of Texture.....	9
1.2.4.3. Effect of Clay content.....	11
1.3. ELECTROMAGNETIC AND RESISTIVITY METHODS THEORY.....	12
1.3.1. Electrical Resistivity Method.....	12
1.3.1.1. Wenner.....	14
1.3.1.2. Dipole-Dipole.....	15
1.3.1.3. Wenner- Schlumberger.....	15
1.3.1.4. Pole-Pole.....	17
1.3.1.5. Pole-Dipole.....	18
1.3.2. Electromagnetic Methods.....	19
1.4. CHARACTERIZATION AND GEOLOGICAL CONTEXT OF THE STUDY AREA.....	22
1.4.1. Area 1 and 2 – Detection of contaminated groundwater.....	22
1.4.1.1. Characterization.....	22
1.4.1.2. Geological context.....	22
1.4.2. Area 3 - Engineering and geotechnical proposes.....	24

1.4.2.1. Characterization.	24
1.4.2.2. Geological context.....	24
1.5. DATA ACQUISITION METHODOLOGY.	26
1.5.1. Electric Resistivity Tomography (ERT).	26
1.5.1.1. Equipment.	26
1.5.1.2. Acquisition.	27
1.5.2. Time-Domain Electromagnetic (TDEM).....	31
1.5.2.1. Equipment.	31
1.5.2.2. Acquisition.	32
1.5.3. Frequency-Domain Electromagnetic (FDEM).....	34
1.5.3.1. Equipment.	34
1.5.3.2. Acquisition.	35
1.6. DATA PROCESSING.....	38
1.6.1. ERT – RES2DINV program.	38
1.6.2. TDEM – TEM-RESEARCHER program.	39
1.7. RESULTS.....	42
1.7.1. Location of contaminated waters.	42
1.7.2. Engineering and geotechnical purposes.	45
1.8. CONCLUSIONS.....	49
2. APPARENT CONDUCTIVITY CALCULATION AND OPTIMIZATION IN FDEM-8.....	51
2.1. INTRODUCTION.....	51
2.2. APPARENT CONDUCTIVITY DEFINITION.....	52
2.3. APPARENT CONDUCTIVITY (σ_a) IN OPTIMIZATION.....	52
2.4. NON-LINEAR INVERSION OF FDEM DATA.....	55
2.5. RESULTS.....	56
2.6. CONCLUSIONS.....	60
3. REFERENCES.....	61

I. List of Figures

Figure 1. Link between material and geophysical properties (adapted from Near-Surface Geophysics, Butler, 2005).	7
Figure 2. Typical range of conductivities and resistivities of geological materials (adapted from Near-Surface Geophysics, Butler, 2005).	10
Figure 3. Schematic representation of ions adsorbed on clay particle (adapted from Resistivity and Induced Polarization Methods. Ward, 1990).	11
Figure 4. Equipotential and current lines for a single current electrode, (adapted from Loke, 2012).	13
Figure 5. Equipotential and current lines for a pair of current electrodes, (adapted from Heen and Muhsen, 2016).	13
Figure 6. Wenner electrodes configuration.	14
Figure 7. Dipole-Dipole electrodes configuration.	15
Figure 8. (I) – Wenner and Schlumberger electrodes configuration. (II) – Pseudo-section patterns for the Wenner and Schlumberger arrays. (Adapted from Loke, 2012).	16
Figure 9. Wenner-Schlumberger electrodes array sensitivity values for n=1 (above) and n=6 (below). (Adapted from Loke, 2012).	17
Figure 10. Pole-pole electrodes configuration.	18
Figure 11. Pole-dipole electrodes configuration.	18
Figure 12 Evolution in depth of the primary (Hp) and secondary (Hs) magnetic fields, for TDEM (adapted from Monteiro Santos, 2006).	19
Figure 13. Primary (Hp) and Second (Hs) magnetic field distribution for a magnetic dipole, in FDEM. Tx – Transmitter; Rx – Receiver. (Adapted from Monteiro Santos, 2006).	20
Figure 14. A) TDEM loops configuration, where Tx and Rx are the transmitter and the receiver, respectively; (I) – The transmitter and the receiver are in central loop; (II) – The transmitter and the receiver are coincident or the same; (III) – The transmitter and the receiver are laterally next to each other, (Adapted from Monteiro Santos, 2006). B) FDEM loops configuration; HCP – Horizontal coplanar; PERP – Perpendicular loop; VCP – Vertical coplanar; VCX – Vertical co-axial, (Adapted from Near-Surface Geophysics, Butler, 2005).	21
Figure 15. Location of the geophysical profiles (P1 and P2), and geological sketch of the study area [Modified from Geological Cartography – Laboratório Nacional da Energia e Geologia (LNEG)].	23
Figure 16. Location of the geophysical profiles inside the study area (below) and geological sketch of Area 3 (above).	25
Figure 17. Syscal Pro Switch instrument (left) with a 90m coil (right) and a connection cube for coils.	26
Figure 18. Creation and configuration of the reading sequence, Electro Pro Software.	28
Figure 19. Graph of the readings. Each dot represents a data point and the different colors represent the levels, which are defined through the space between MN electrodes, Electro Pro Software.	28

Figure 20. Extended coil with the main Unit (left) and installation of the electrodes and connections (right).	29
Figure 21. Left – Second reading; Right – Third reading. AB – Current electrodes; MN – Potential electrodes; Black dot – Reading. The colors represent measurement levels.	30
Figure 22. Data transfer using the Proxys II software.	30
Figure 23. TDEM acquisition device, (adapted from www.aerm.net).....	31
Figure 24. TEM-FAST 48 HPC parameters; Left – For 50m x 50m loops; Right – 25m x25 m.	33
Figure 25. All components of the TEM-FAST connected to the main unit.	33
Figure 26. FDEM-8 (Des Barlow) – Coils (red), transmitter (right) and receiver (left).	34
Figure 27. FDEM-8 setup menu.	35
Figure 28. FDEM-8 sounding assembled.	36
Figure 29. Different formats of data conversion in PCFDEM software.	37
Figure 30. Example of the Profile in Area 1 – Correction of the bad data points in RES2DINV software, for the profile in Area 1.	38
Figure 31. Example of the Profile in Area 1 – From top to bottom; measured apparent resistivity; calculated apparent resistivity and the inverse model.	39
Figure 32. Example of one sounding of the Profile in Area 3 – Edit and smoothing field data in TEM-RES.	40
Figure 33. Example of one sounding forward model creation in TEM-RES – A model with 3 layers.	41
Figure 34. Cross-section creation in TEM-RES software.....	41
Figure 35. Results from Profile 1. ERT (bottom), FDEM (Top). Location of contaminated groundwater (C1-C2). The FDEM depth is represented in the ERT profile by the grey line.	43
Figure 36. Results from Profile 2. ERT (bottom), FDEM (Top). Location of contaminated groundwater (C1-C2). The FDEM depth is represented in the ERT profile by the grey line.	44
Figure 37. Results from Profile 1. ERT (bottom), FDEM (Middle) and TDEM (Top). The layers are represented by red lines (L1, L2, and L3). Engineering and geotechnical purposes.	46
Figure 38. Results from Profile 2. ERT (bottom) and TDEM (Top). The layers are represented by red lines (L1, L2, and L3). Engineering and geotechnical purposes.	47
Figure 39. Results from Profile 3, ERT. Location of resistive bodies (R1-R2). Black vertical dashed lines – Possible faults. Black vertical lines – Interception with P1 and P2. Engineering and geotechnical purposes.	48
Figure 40. FDEM inversion from a nonlinear smoothness-constrained least square method; A - for 8 iterations and a Lagrange parameter =0.3; B – for 19 iterations and a Lagrange parameter = 3; C – for 31 iterations and a Lagrange parameter = 30.	57
Figure 41. FDEM inversion from a nonlinear smoothness-constrained least square method; A - for 23 iterations and a Lagrange parameter =3; B – for 34 iterations and a Lagrange parameter = 30.	58
Figure 42. FDEM inversion from a nonlinear smoothness-constrained least square method; A - for 22 iterations and a Lagrange parameter =3; B – for 31 iterations and a Lagrange parameter = 30.	59

II. List of Tables

Table 1. Output Current for the different frequencies in FDEM-8.....	37
--	----

1. COMBINING ERT, TDEM, AND FDEM IN SHALLOW GEOPHYSICAL INVESTIGATION.

1.1. Introduction

1.1.1. Thesis Framework.

For decades, geophysical methods have been applied in the exploration of hydrocarbons, groundwater, and large ore deposits [McNeill (1980), Orange (1989)]. However, in recent years this application has spread to environmental and agricultural areas [Benson, (1995); Mota *et al.* (2004); Sharma and Baranwal (2005); Monteiro Santos (2006)]. The increasingly accelerated demand for irrigated groundwater due to the increase in crops, the location of contaminants in groundwater and identify pathways for contaminant transport, leads to an increasing demand for geophysical prospecting.

In that context, shallow geophysical investigation or near-surface geophysics uses the physical principles and relations to study the physical properties of the uppermost part of the earth's crust. There are numerous and varied application fields where geophysical investigation is used, such as:

- ◆ Engineering geology and geotechnical.
- ◆ Environmental.
- ◆ Groundwater exploitation.
- ◆ Mining.
- ◆ Archaeological.

Such fields are characterized by a wide range of depths depending on the target, shallow (archaeological) to deep (mining). In addition, for each of them, there are other issues that must be considered: resolution requirements, either vertical or horizontal. As an example: if the intention is to locate faults and fractures in a low permeability bedrock searching for water, an error in horizontal and vertical resolution can lead to a dry hole. Near real-time validation, since geophysical methods are indirect methods it's always needed verification or validation of geophysical survey results and interpretation. In some cases this validation can be immediately executed excavating a trench, in other cases, this validation may not occur for weeks or months.

Electrical and electromagnetic methods are the only geophysical methods that are directly influenced by the electric properties of pore fluid and they are very sensitive to changes in geology such as lithology, porosity, grain size, fractures, and clay content.

Thus, it is essential to know what kind of method should be used in each area. In this work, Electrical Resistivity Tomography (ERT), Time-Domain Electromagnetic (TDEM) and Frequency-Domain Electromagnetic (FDEM) methods were used, all linked to groundwater studies and their application in engineering geology, geotechnical and environmental studies. These methods are well recognized for mapping shallow and deep structures as image aquifers, (Gonçalves *et al.* 2017).

For Engineering and geotechnical purposes, the application of ERT, TDEM, and FDEM is known but poorly used, although the great potential of these methods for defining subsurface details with a high level of accuracy, precision, cost efficiency, and safety. In fact, geophysical methods can be used for the characterization of geological structures, stratigraphy, as well as to improve the conditions associated with the drilling processes. This might be particularly important due to the major part of exploration or characterization costs are spent in drilling and sampling.

Moreover, the current use of the FDEM method with the equipment FDEM-8 is in a qualitative domain, which means that a model of resistivity distribution is not used in data interpretation.

The overarching goal of the present study is based on the comparison of the models and results for the three geophysical methods applied over the same profiles: ERT, TDEM, and FDEM. For this purpose these methods have been used in two different cases of study: determining the location of contaminated groundwater due to mining activity derived from mineral separation processes –meaningful to monitoring impacts to the environment and for the health of people around sites– and provide critical information about subsidence potential and bedrock geometry for engineering and geotechnical proposes.

In addition, there is a second major objective focused on the transformation of the usual qualitative representations of the FDEM-8 data into a quantitative one by calculating the resistivities of the subsurface by inversion. This transformation will allow comparing the results of the FDEM with the model of ERT and TDEM.

1.1.2. History and state-of-art of Applied Geophysics.

Electrical resistivity surveys have been used for decades in hydrogeological, mining, geotechnical, environmental and even hydrocarbon exploration.

The initial chronology of Electrical Resistivity dates back to the late 19th century, with the works of Fox (1830), Kelly (1835) and Barus (1882) in observing electrical currents in deposit of copper and sulfites. But it was at the beginning of the twentieth century, through the introduced direct current equipotential line method by Conrad Schlumberger (1912) to map a metallic deposit at the Sain-Bel mines in France, - that the first approach to electrical methods in mining was applied in a practical context.

Later, Wenner (1912) and Schlumberger (1920) introduced the concept of apparent resistivity, leading to a development of the equipments for apparent resistivity acquisition. Several arrays for measuring the potential difference between electrodes have been used. Wenner employed the equal-spaced electrode array

(Wenner array). Schlumberger applied an electrode configuration in which the potential electrodes are sufficiently close that the electric field is measured between the current electrodes (the Schlumberger array). The gradient array is a modified Schlumberger array developed for multichannel equipment. More specifically, in the gradient array, the current electrodes are farther apart and the potential electrodes are moved in-line between the current electrodes. There are other types of array that will be explained in chapter 1.2, which have different approaches and produce different results.

From 1920s to 1970s, electrical prospecting was developed and applied to geological issues, with several limitations in both measurement equipment and interpretation strategies. In the late 1970s, the increase in computation development allowed new modeling methods leading to studies for medical diagnostics and showed that geophysical electrostatic (or galvanic) electrical imaging was possible, with Lytle and Dines (1973) and Daily and Owen (1990).

In 1993, Griffiths and Barker applied two-dimensional resistivity imaging and modeling in areas of complex geology. This improvement allowed to draw conclusions regarding the depth of investigation and electrode spacing, increasing the rate of data acquisition and providing satisfactory images from the field data after an automatic inversion.

The development of the electromagnetic method was largely dormant in the interval 1930-50, despite prior attempts by Matteucci (1867). The applicability of electromagnetic methods came a few years later compare with electrical methods, with Schlumberger (1920) decaying polarized induction. However, it was in the following 30 years that the greatest developments arrived mainly due to the theoretical works of Wait (1951-1958).

A description of a time-domain electromagnetic was provided by Kaufman and Keller (1983) giving the development of the theory of the asymptotic behavior of electromagnetic fields in layered media.

In 1988, Nabighian published three-volume work on applied electromagnetic methods, which have been considered the most comprehensive work available - at the time. It covered theory, field methods, and data interpretation management, further extending the work already done by Ward (1967) and, providing practical and useful information on electromagnetic methods.

Since the twentieth century, geophysical methods have been increasingly used in the investigation of groundwater and contaminated areas. Among some works is McNeill's (1990) with a review of the use of electromagnetic methods for groundwater studies contributing to the development of this field of research.

In 1995, Benson *et al.* mapped the groundwater contamination using resistivity and electromagnetic geophysical methods. In 2000, Abdul Nassir *et al.* mapped a salt-water intrusion by geo-electrical imaging surveys. Mota *et al.* (2004) applied geo-electrical surveys to detected incipient pollution beneath a recent landfill. Sharma and Baranwal (2005) used both electric and electromagnetic methods in a delineation of groundwater - bearing fracture zones while Monteiro Santos (2006) mapped the groundwater contamination around a landfill facility using electromagnetic methods.

Many other studies have contributed to the development and applicability of electric and electromagnetic methods in environmental issues.

1.2. Properties of Near-Surface Soils

Maxwell's equations provide the starting point to obtain an understanding of the application of electric and magnetic fields for studying the structure of the earth, as well as to determine its properties. The equation that represents the fact that magnetic fields are caused by electrical current flow is:

$$\nabla \vec{H} = \vec{J} + \frac{\partial \vec{D}}{\partial t} \quad (1.2.1)$$

Where H is the magnetic field vector, J is the current density vector and D is the electric displacement vector. This equation represents two kinds of current flow, one (J) in which charge carriers flow through a medium without obstacles, and another $\frac{\partial \vec{D}}{\partial t}$ in which charge separation, and hence an impeding electric field, arises. The first type of current is often called ohmic, or galvanic.

A second equation, called Faraday's law, which describes the creation of an electric field by a time-varying magnetic field, can be written;

$$\nabla \vec{E} = -\frac{\partial \vec{B}}{\partial t} \quad (1.2.2)$$

Where E is the electric field vector and B is the magnetic induction vector. These two Maxwell's equations characterize the electromagnetic field behavior for any application in geophysical exploration.

However, it is necessary to relate the behavior of the change in the electromagnetic field to the subsurface structure or its properties. Those relationships are called constitutive equations, (Keller, 1988).

1.2.1. Electric Properties

The most important of the constitutive equations in terms of inductive methods of geophysical prospecting is the Ohm's law. The effective electrical conductivity σ of a material is a property that quantifies the relationship between the applied electric field E and a density of current J that runs through the volume unit of this material. It can be expressed for a linear homogeneous and isotropic material:

$$\vec{J} = \sigma \vec{E} \quad (1.2.3)$$

Since both electric field E and the current density are vectors, the quantity σ must be a tensor, which can be written in Cartesian coordinates:

$$\sigma = \begin{bmatrix} \sigma_{xx} & \sigma_{xy} & \sigma_{xz} \\ \sigma_{yx} & \sigma_{yy} & \sigma_{yz} \\ \sigma_{zx} & \sigma_{zy} & \sigma_{zz} \end{bmatrix} \quad (1.2.4)$$

If two of the orthogonal coordinate directions are selected, the conductivity tensor has a simple form which lie in the direction of maximum conductivity and minimum conductivity (the principal directions of the conductivity tensor):

$$\sigma = \begin{bmatrix} \sigma_{xx} & 0 & 0 \\ 0 & \sigma_{yy} & 0 \\ 0 & 0 & \sigma_{zz} \end{bmatrix} \quad (1.2.5)$$

For isotropic materials the principal values of conductivity are equal and the electrical conductivity is a scalar. In this type of material, the current density and electric field vectors are collinear. For anisotropic materials the main values are different, and they only can be collinear if the applied electric field is in the direction of one of the tensor principal directions, (Keller, 1988).

The response of a material to an applied electrical field can be represented by the effective electrical conductivity, which represents the real part of the electric conductivity and is the measure reported from field studies. In general, the response is not represented by a real quantity and it is not constant, instead is a complex function of frequency:

$$\sigma = \sigma'(w) - i\sigma''(w) \quad (1.2.6)$$

Where $w = 2\pi f$ is the angular frequency, f is the frequency, $\sigma'(w)$ and $i\sigma''(w)$ are the real and imaginary part of the electric conductivity ($i = \sqrt{-1}$).

When referring to resistivity methods, it's convenient to use the concept of effective electric resistivity (ρ). Hence, the equation 1.2.6 become:

$$p = p'(w) - ip''(w) \quad (1.2.7)$$

The real and the imaginary parts of the electric conductivity are related to the electric resistivity through:

$$\rho' = \frac{\sigma'}{|\sigma|^2} \quad (1.2.8)$$

$$\rho'' = \frac{\sigma''}{|\sigma|^2} \quad (1.2.9)$$

As it is referred in some cases, and for the most commonly used frequency range in geo-electromagnetic studies, electrical conductivity may be represented by a scalar. Therefore the inverse magnitude, i.e. the effective electrical resistivity, can be defined by:

$$\rho = 1/\sigma \quad (1.2.10)$$

These components of the imaginary and real parts are very important. Borner *et al.* (1993) found that the imaginary component of electrical conductivity is particularly sensitive to the presence of contamination, having Park and Dickey (1989) found that this component is also sensitive to the presence of clay.

1.2.2. Electromagnetic properties

The electromagnetic properties of the earth components include the magnetic permeability μ , which is the ability of the medium to respond to a magnetic field, the dielectric permittivity ϵ , the ability of the soil to become polarized in response to an electric field, and the electric conductivity σ , mentioned in last section.

The dielectric permittivity is related to electric field, for a linear homogenous half-space, according to;

$$D = \epsilon \vec{E} \quad (1.2.11)$$

Where D is the electric displacement and E is the electrical field. As the electrical conductivity, dielectric permittivity is a tensor and it is also a complex frequency-dependent parameter, defined as following after the sign convention adopted by Ward and Hohmann (1988);

$$\epsilon(w) = \epsilon'(w) - i\epsilon''(w) \quad (1.2.12)$$

The third electromagnetic property or constitutive equation is the magnetic permeability (μ) which relates the magnetic field strength to the magnetic induction (B) and it is written as:

$$B = \mu \vec{H} \quad (1.2.13)$$

This property constitutes the basis for the magnetic methods in geophysical exploration, but also plays an essential role in the electromagnetic methods.

Like conductivity and dielectric permittivity, magnetic permeability is a tensor quantity. However, in contrast to the other two properties, which are usually considered independent of applied field strengths at the levels used in exploration, magnetic permeability can have a complicated dependence on magnetic field strength. If no material is present, a free-space relationship exists between field strength and induction:

$$B = \mu_0 \vec{H} \quad (1.2.14)$$

Where μ_0 is the magnetic permeability of the free space. This defines an important quantity for use in calculations of electromagnetic field behavior, (Keller, 1988).

1.2.3. Electronic, Semi-Conductive and Electrolyte Conduction.

The ground resistivity is related to several geological parameters such as the mineral and fluid content, porosity, permeability and degree of water saturation in the rock (Fig. 1).

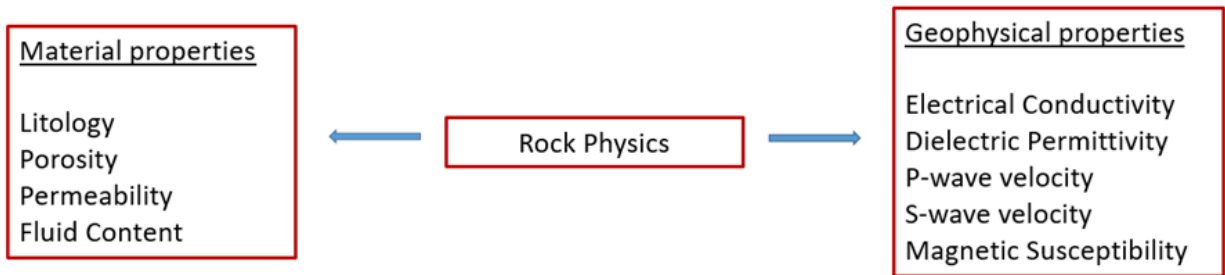


Figure 1. Link between material and geophysical properties (adapted from Near-Surface Geophysics, Butler, 2005).

1.2.3.1. Electronic Conduction.

There are several physical processes that allow the electrical conduction on a rock. Classification in electrolytic, electronic and semi-conductive conduction reflects only the dominant mechanism.

The electronic conduction corresponds to metals and is classified and explained by the Drude theory, which says that there are clouds of electrons in permanent and disorganized movement called valence electrons. When an external electrical field is applied, the electron cloud acquires an organized movement originating an electric current as defined by:

$$\sigma = ne^2\tau/m \tag{1.2.15}$$

Where n is the number of free electrons for a metal volume unit; e is the electron electrical charge; m is the electron mass and τ is the relaxation time. The organized movement is occasionally perturbed by clashes between electrons. The average time between the clashes is called relaxation time, and this parameter is highly influenced by temperature. Increasing temperature decreases conductivity because increases network vibration and therefore decreases relaxation time (Monteiro Santos, 2006).

1.2.3.2. Semi-conductive Conduction.

In the semi-conductive conduction, the valence electrons can only be released by thermal action. When an electron is released, a gap is created. This gap can be occupied by neighboring electrons, resulting in a gap movement. This movement is highly influenced by temperature according to Stefan-Boltzmann law (Monteiro Santos, 2006);

$$n_e \propto \exp(-E/kT) \quad (1.2.16)$$

Where, n_e is the number of electrons, E is the activation energy (characteristic of each material), k is the Boltzmann constant and T is the absolute temperature. Unlike electronic conduction, the electrical conductivity of semiconductors increases with temperature.

The geological materials, excluding pure metals, generally behave as semiconductors. If the activation energy is low, the materials behave as conductors, like sulfites. If the activation energy is high the material behaves as an insulator, like silicates where minerals have high activation energy values. In these materials, ionic conduction is more important than electronics.

1.2.3.3. Electrolytic Conduction.

The resistivities from near-surface rocks are generally restricted by electrolytic conduction by pores, fractures, faults and shear zones. Since each ion is able to carry only a certain quantity of charge, it follows that the more ions that are available in a solution the greater will be the charge that can be carried. Hence, the solution with a larger number of ions will have a higher conductivity or less resistivity (Ward, 1990).

When salt dissolves in water, the ions (positive and negative) separate and become free to move in the liquid. In the absence of an electric field, this movement is random and the solution is presented as electrically neutral. In the presence of an external electric field, the anions will move in the direction of the applied field and the cations in the opposite direction, allowing the passage of electric current (Monteiro Santos, 2006).

However, there are some effects that influence the electrolyte conduction: temperature, rock texture, and porosity, rock type, geological processes and presence of clay minerals.

1.2.4. Effects on Electrolyte Conduction.

1.2.4.1. Effect of Temperature.

An increase in temperature decreases the viscosity of water, increasing the electrons mobility which results in an observed resistivity fall (Keller and Frischknecht, 1966);

$$\rho_t = \rho_{18} / [1 + \alpha(t - 18)] \quad (1.2.17)$$

Inversely for conductivity;

$$\sigma_t = [1 + \alpha(t - 18)]\sigma_{18} \quad (1.2.18)$$

Where ρ_{18} and σ_{18} represent respectively the electric resistivity and conductivity at 18°C, α is the temperature coefficient of resistivity (0.025 per 1°C on average) and t is the ambient temperature.

These empirical expressions can explain the behavior of water's electrical conductivity and resistivity with temperature.

1.2.4.2. Effect of Texture.

The conductivity of the rock matrix is very variable and depends on its texture and anisotropy. In an isotropic matrix with a random porous structure, the conductivity does not depend on the direction in which the measurement is made. If the pore shape has preferential directions, then the electrical conductivity varies with the measuring direction.

On the one hand, a well-sorted sandstone has large void spaces and hence exhibits low resistivity while a poorly sorted sandstone will have much lower porosity and hence will exhibit higher resistivity (Fig. 2). On the other hand, dissolution along fractures in limestone will enhance porosity and hence lower resistivity, as the precipitation of some minerals in any rock will lower the porosity and consequently increase resistivity (Ward, 1990).

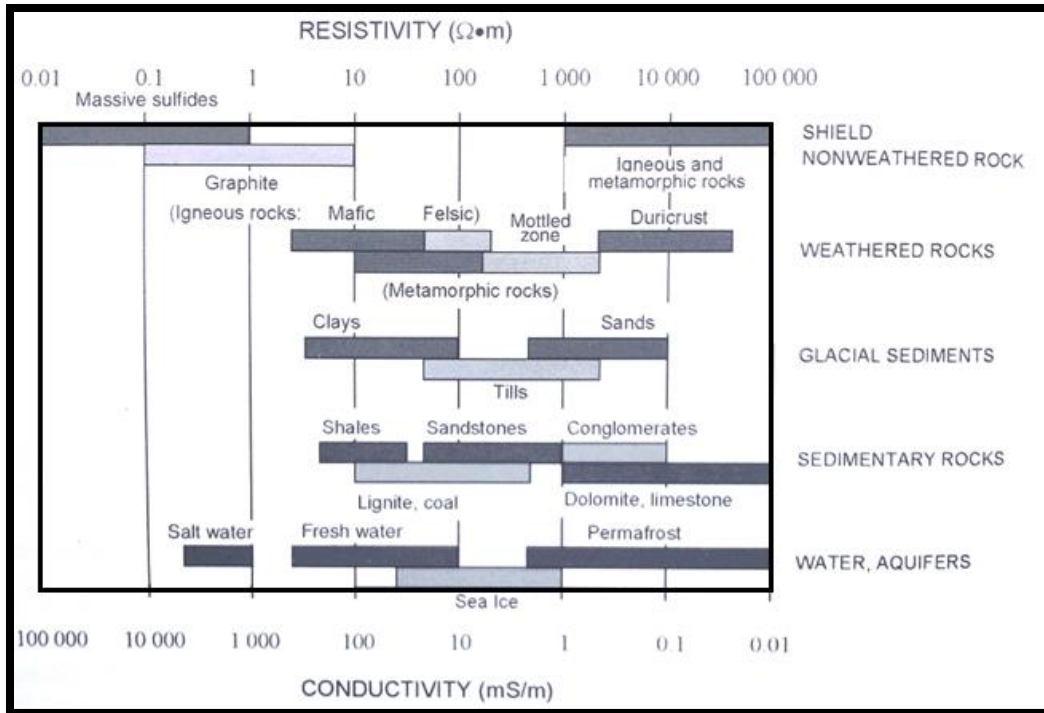


Figure 2. Typical range of conductivities and resistivities of geological materials (adapted from Near-Surface Geophysics, Butler, 2005).

Summarizing the Fig. 2 as follow:

- ◆ In sedimentary rocks, the resistivity is lower when compared with other types of rocks. However some of these rocks can reach higher resistivities essentially because they are dry - Within this group, there are dune sands and those with very low porosity such as plaster;
- ◆ In eruptive rocks, due to their low porosity, values of resistivity are high and may increase with the appearance of fractures. However, for new magmas the value of resistivity it's not so high, increasingly with the decompression over time.
- ◆ Metamorphic rocks present values of electrical conductivity that are between the values of sedimentary and the eruptive rocks. Because porosity and water content depend on the degree of metamorphism, the effective electrical resistivity increases with metamorphism. However, there are some exceptions that change the electric resistivity in this type of rock. For example, the presence of graphite increases the electronic conduction hence increasing electrical conductivity.

1.2.4.3. Effect of Clay content.

The effect of clay content is more complex than the other effects and sometimes causes major problems in data interpretation. The presence of clay in a geological context has two effects with respect to its geoelectric behavior: on the one hand, it decreases the electrical resistivity of the medium and, on the other hand, makes this property dependent on the frequency of the electromagnetic field (Monteiro Santos, 2006).

The origin of the unusual high clay mineral conductivity lies in a double layer of cation exchange. Cations are required to balance the charge due to substitution within the crystal lattice. The finite size of the cations prevents the formation of a single layer. Rather, a double layer is formed which consists of a fixed layer immediately adjacent to the clay surface and a diffuse layer which drops off in density exponentially with distance from the fixed layer, (Fig. 3) (Ward, 1990).

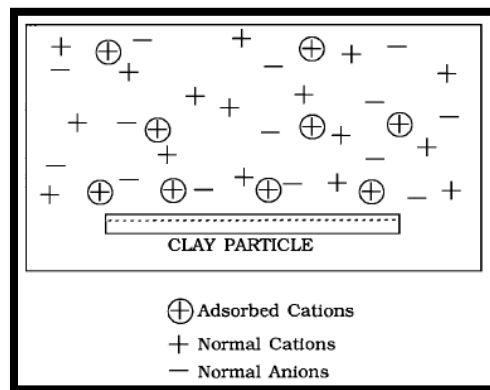


Figure 3. Schematic representation of ions adsorbed on clay particle (adapted from Resistivity and Induced Polarization Methods. Ward, 1990).

The diffusion layer, due to the large number of ions, has a capacity for conduction of electric current higher than the fluid that normally fills the pores of the rock formation and therefore represents a parallel (and more efficient) path for conducting the electrical current. As clay particles have a large useful area, the presence of mineral in rocks, together with the presence of water, significantly changes the conductivity of the rock formation (Monteiro Santos, 2006).

The purpose of electrical and electromagnetic surveys is to determine the subsurface resistivity distribution by making measurements on the ground surface. From these measurements, the resistivity of the subsurface can be estimated. For that, is necessary to investigate the relationship between material and geophysical properties.

The analysis of the physicals properties of the rock allows developing a major understanding of the relationship between material and geophysical properties. There are two ways for analysing the physical properties of the rocks in geophysics: forward and inverse process. Forward models define the physical

properties of the subsoil and calculate the geophysical response. Inverse models calculate the physical properties through the data measured on the field to obtain the geological response (Butler, 2005).

The principal difference between these two approaches is the redundancy of the inverse problem, in the sense that many combinations of material properties that can produce the same geophysical property for a given material, unlike forward problem which will predict a unique geophysical response for a given material, i.e. in the forward model it is obtained a unique geological model while in the inverse process numerous geological models are found (Butler, 2005).

1.3. Electromagnetic and Resistivity Methods Theory.

1.3.1. Electrical Resistivity Method.

Electrical geophysical methods are also called galvanic source methods, by directly coupling or injecting electrical current into the ground via electrodes. For the typical resistivity method, the source used is a low frequency ‘current generator’. Since the frequencies used are low, the theory corresponding to ‘direct currents’ is valid (Butler, 2005).

Consider a point source of direct current of intensity I on the surface of isotropic, homogeneous infinite half-spaced of electrical resistivity or conductivity;

$$I = \iint \vec{j} \cdot \vec{n} ds \quad (1.3.1)$$

Since the electric field is very low frequency, it can be represented by the electric potential V :

$$\vec{E} = -gradV \quad (1.3.2)$$

For a single point, the current flows radially away from the source and the potential varies inversely with distance from the current source (Fig. 4). If the current is injected in a point at the earth's surface, the equipotential surfaces have a hemisphere shape, and the current flow is perpendicular to the equipotential surface. In this case, the potential is given by:

$$V = \frac{\rho I}{2\pi r} \quad (1.3.3)$$

Where r is the distance of a point in the medium from the electrode. In practice, all resistivity surveys use at least two current electrodes, a positive one and a negative one:

$$V = \frac{\rho I}{2\pi} \left(\frac{1}{r_A} - \frac{1}{r_B} \right) \quad (1.3.4)$$

To use electric current in the ground investigation, four electrodes are used conventionally: an electric field of direct current through two current electrodes (A, B) connected to a milliAmperimeter; and two potential electrodes (M, N) connected to a milliVoltmeter. With this device, the difference in electrical potential ΔV is measured between points M and N and the current intensity between A and B, from which can be calculated the value of apparent or theoretical resistivity, (Fig. 5).

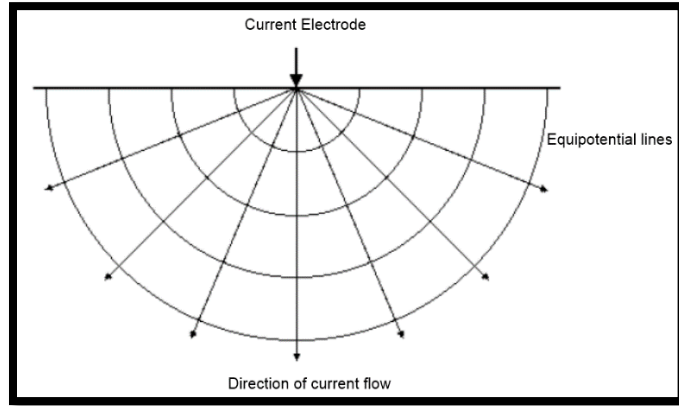


Figure 4. Equipotential and current lines for a single current electrode, (adapted from Loke, 2012).

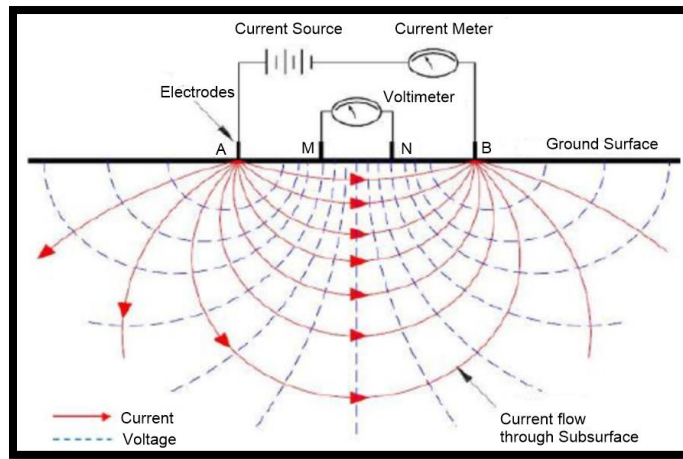


Figure 5. Equipotential and current lines for a pair of current electrodes, (adapted from Heen and Muhsen, 2016).

This voltage difference or potential difference can be written as follow:

$$\Delta V = V_M - V_N = \frac{I\rho}{2\pi} \left(\frac{1}{AM} - \frac{1}{AN} - \frac{1}{BM} + \frac{1}{BN} \right) \quad (1.3.5)$$

Where AM, AN, BM and BN are the distances in meters between the current and the potential electrodes. The resistivity calculated by the equation (1.3.5) corresponds to the apparent resistivity of the ground and is not the real resistivity. This is because the ground is usually heterogeneous so that the electric field introduced into the ground affects simultaneously to various layers and the measured resistivity corresponds to an intermediate value of all of them. The measured value of resistivity coincides with the real resistivity only in homogeneous soils or very shallow depths of investigation. From measurements of apparent resistivity, the real resistivity of different materials is obtained by the inversion process.

From the current (I) and the potential difference (ΔV) values, an apparent resistivity can be calculated:

$$\rho_a = K \frac{\Delta V}{I} \quad (1.3.6)$$

And,

$$K = 2\pi \left(\frac{1}{AM} - \frac{1}{AN} - \frac{1}{BM} + \frac{1}{BN} \right)^{-1} \quad (1.3.7)$$

Where K is the geometric factor that depends on the arrangement of the four-electrode system.

There are several measurement arrays that can be used in electric methods. This array together with the profile length determines the depth of investigation.

1.3.1.1. Wenner.

Many of the early 2-D surveys were carried out with this configuration. For a four-electrode array, there are three possible permutations in the positions of the electrodes. The Wenner array is relatively sensitive to vertical changes in the subsurface resistivity below the center of the array. However, it is less sensitive to horizontal changes in the subsurface resistivity. (Loke, 2012). In other way, among common arrays has the strongest signal strength, which is inversely proportional to the geometric factor used to calculate the apparent resistivity value:

$$\rho_a = 2\pi a \frac{\Delta V}{I} \quad (1.3.8)$$

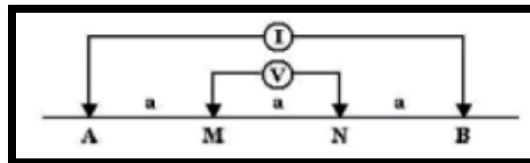


Figure 6. Wenner electrodes configuration.

1.3.1.2. Dipole-Dipole.

The great advantage of this array is the low electromagnetic coupling between the current and the potential circuits. For this reason, this is one of the most used arrays in resistivity and induced polarization (IP) method.

The spacing between the pair of current electrodes (A, B) is the same that the potential one (M, N), defined with parameter 'a' (Fig. 7). The distance between the pair of electrodes is defined as 'na'.

The 'a' spacing is fixed at the smallest unit electrode spacing and the 'na' factor is increased from 1 until up to about 6 in order to increase the depth of investigation.

This type of configuration is very sensitive to horizontal resistivity changes but relatively less sensitive to vertical ones. This is due to the fact that the largest sensitivity values are located between the current electrodes (A, B) as well as between the potential electrodes (M, N). Thus, it works well for detecting lateral changes, such as dikes and cavities, but relatively poorly in mapping horizontal structures such as sills or sedimentary layers. Compared with the Wenner array, dipole-dipole has a shallower depth of investigation (Loke, 2012).

The apparent resistivity is then calculated:

$$\rho_a = \frac{\Delta V}{I} \pi a n(n+1)(n+2) \quad (1.3.9)$$

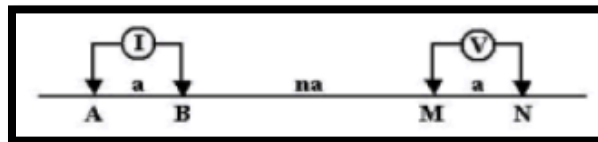


Figure 7. Dipole-Dipole electrodes configuration.

1.3.1.3. Wenner- Schlumberger.

This array combines the Wenner and Schlumberger traditional arrangements. The traditional Schlumberger array is one of the most commonly used arrays for resistivity surveys, and it is characterized by the higher space between current electrodes (A, B) in relation to the space between potential electrodes (M, N), which leads to sensitivity pattern for horizontal and vertical resistivity variations [Fig. 8 (I); (Loke, 2012)].

Here, the sensitivity pattern becomes more concentrated beneath the potential electrodes (M, N) as the 'n' factor is increased from 1 (Wenner array) to 6 (the classical Schlumberger array), as can be seen in Figure 9.

At $n=6$, the high positive sensitivity lobe beneath the M and N electrodes becomes more separated from the high positive sensitivity values near the A and B electrodes. Analyzing means that this array is moderately sensitive to both horizontal (for low 'n' values) and vertical structures (for high 'n' values) (Loke, 2012).

The electrodes configuration can be seen in Figure 8 as well as the pseudo-section patterns for both arrays. It shows that the Wenner-Schlumberger array has a slightly better horizontal coverage compare with the Wenner array. For the Wenner array, each deeper data level has 3 data points less than the previous data level, while for the Wenner-Schlumberger array there is a loss of 2 data points with each deeper data level.

In areas where both types of geological structures are expected, this type of array might be a good compromise between the Wenner and the dipole-dipole array (Loke, 2012). The apparent resistivity for Schlumberger array can be calculated as follow:

$$\rho_a = \frac{\Delta V}{I} \pi \frac{b^2}{a} \quad (1.3.10)$$

Where the deep of exploration is greater than $\frac{AB}{8}$ for both Wenner and Schlumberger arrays (Butler, 2005).

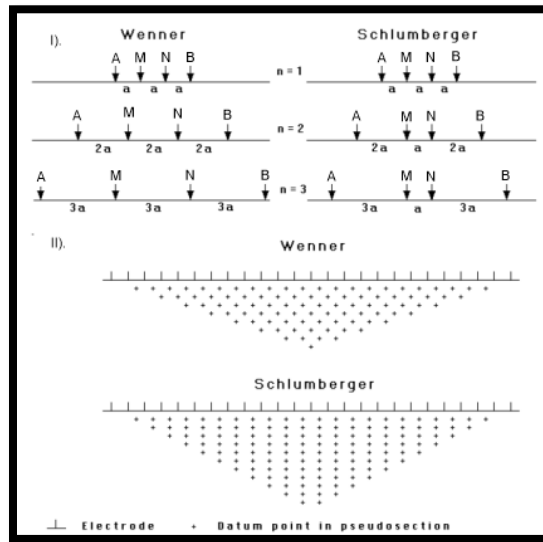


Figure 8. (I) – Wenner and Schlumberger electrodes configuration. (II) – Section patterns for the Wenner and Schlumberger arrays. (Adapted from Loke, 2012).

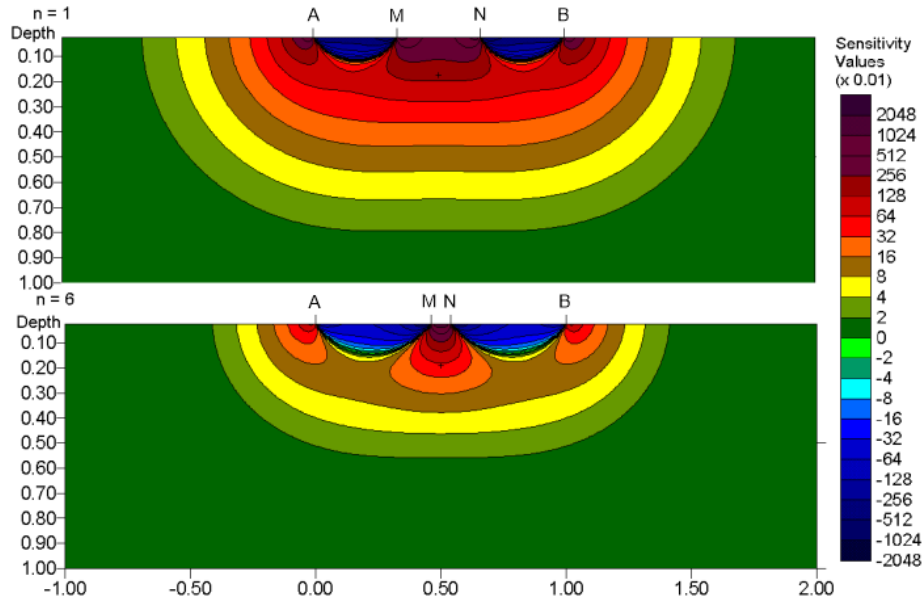


Figure 9. Wenner-Schlumberger electrodes array sensitivity values for n=1 (above) and n=6 (below). (Adapted from Loke, 2012).

1.3.1.4. Pole-Pole.

Unlike the devices already mentioned, pole-pole array is not so commonly used. In practice, the ideal pole-pole array, as shown in Figure 10, with a single current and potential electrode, does not exist. To approximate the pole-pole array, the second current (B) and potential electrodes (N) must be placed at a distance that is more than 20 times the maximum separation between M and A electrodes used in the survey (consider as infinite) to ensure that the error is less than 5%. This creates a problem when the space between electrodes along the survey line is more than a few meters, making it hard to find a suitable location for B and N that satisfy this requirement (Loke, 2012).

Another disadvantage of this array is that because of the large distance between M and N electrodes, it can pick up a large amount of telluric noise that can severely degrade the quality of the measurements. Thus, this array is mainly used in surveys where relatively small electrode spacing (less than a few meters) is used such as archaeological surveys (Loke, 2012). In addition, some of the 3D arrays use the pole-pole configuration.

In this type of array the apparent resistivity can be calculated:

$$\rho_a = 2\pi a \frac{\Delta V}{I} \quad (1.3.11)$$

Having a depth of exploration greater than 2.5 a-spacing and a lateral resolution about $\frac{1}{2}$ a-spacing (Butler, 2005).



Figure 10. Pole-pole electrodes configuration.

1.3.1.5. Pole-Dipole.

The pole-dipole array has an asymmetrical configuration that has a good horizontal coverage with a significantly higher signal strength compared with the dipole-dipole array. Moreover, is not sensitive to telluric noise as the pole-pole array.

Due to its asymmetry, over symmetrical structures, the apparent resistivity anomalies in the pseudo-section are asymmetrical, which could influence the model obtained after inversion. To eliminate the effect of this asymmetry it is necessary to perform forward and reverse measurement along a profile, but this implies double the number of data points and consequently the survey time (Loke, 2012).

For a pole-dipole array is necessary a remote electrode (B) which must be placed sufficiently far from the survey line. The effect of the current electrode (B) is approximately proportional to the square of the ratio of the A-M distance to the B-M distance. Thus, this array is less affected by the B remote electrode compared to the pole-pole array (Loke, 2012).

Compared with Wenner and Wenner-Schlumberger, it has a lower signal strength but higher in relation to the dipole-dipole array.

The apparent resistivity for this array can be written as:

$$\rho_a = 2\pi \frac{(a + b) \Delta V}{b I} \quad (1.3.12)$$

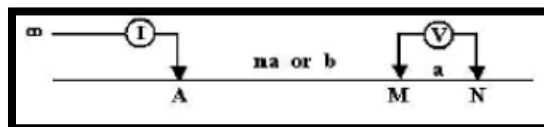


Figure 11. Pole-dipole electrodes configuration.

1.3.2. Electromagnetic Methods.

Electromagnetic methods are inductive methods, as it was mention in section 1.2, eq. 1.2.2. The distribution of the electrical current in the ground diffuses, increasing with time and decreasing with frequency.

There are two types or main divisions of EM inductive methods, Frequency Domain (FDEM) and Time Domain (TDEM).

In TDEM a constant electrical current is injected through a cable generating a primary magnetic field that is in consonance with the electrical current. When the electrical current is cut off, start the decay of the primary magnetic field during the ramp time. According to Faraday's Law (eq. 1.2.2), an electromotive force induces a secondary electrical field in depth, known as eddy current. At the end of the ramp time, the electromotive force diffuses. The secondary magnetic field is generated by the secondary electrical field in consonance with it and with the subsoil resistivities (Fig. 12), (McNeill, 1990).

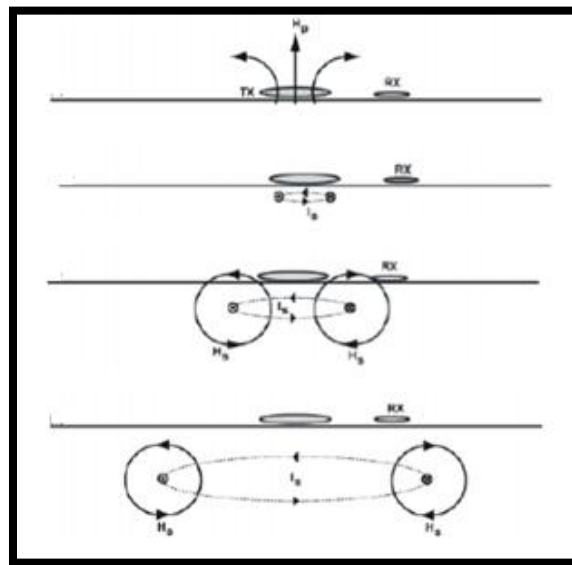


Figure 12 Evolution in depth of the primary (H_p) and secondary (H_s) magnetic fields, for TDEM (adapted from Monteiro Santos, 2006).

For the frequency domain, the variable magnetic field generated in the transmitter (primary field [H_p]) induces electrical eddy currents in the subsoil. These currents create a secondary magnetic field (H_s) in the presence of a conductor, which is measured jointly with H_p in the receiver, (Fig. 13).

The major difference between these two methods is in the source and the receiver, i.e., while in TDEM the transmitter current is generated by pulses, which means the depth reached its time-dependent, in the FDEM

the transmitter current is generated permanently, which means that the depth reached is frequency-dependent. This provides one great advantage to TDEM in measuring the received secondary signal when the stronger primary transmission signal is off and was the main reason for the appearance of TDEM. (Monteiro Santos, 2006)

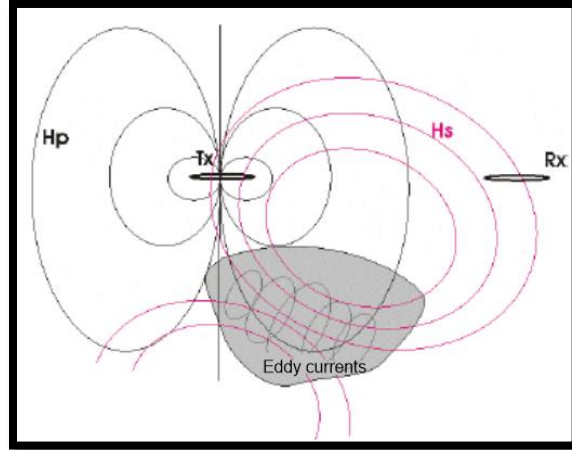


Figure 13. Primary (Hp) and Second (Hs) magnetic field distribution for a magnetic dipole, in FDEM. Tx – Transmitter; Rx – Receiver. (Adapted from Monteiro Santos, 2006).

The loops configuration and the skin effect are important in the investigation depths. The skin depth is the distance which an electromagnetic wave had loss their amplitude by a factor of $\frac{1}{e}$ and can be estimated, for a TDEM:

$$\delta = \left(\frac{2t}{\sigma\mu}\right)^{1/2} \quad (1.3.13)$$

And for FDEM:

$$\delta = \left(\frac{2}{\sigma\mu\omega}\right)^{1/2} \quad (1.3.14)$$

The skin depth is a function of frequency (FDEM) and time (TDEM) and material properties. Thus, for FDEM, during the soundings, the frequencies are variable in order to reach deeper depths. For TDEM variable changed is the time of the wave (Butler, 2005).

The loops configuration, the transmitter, and the receiver, for the TDEM, can be the same coil/wire, this is only possible due to the power on and off of the current, while for the FDEM the transmitter and the receiver are different coils/wires. The loops configuration for both methods can be seen in Figure 14.

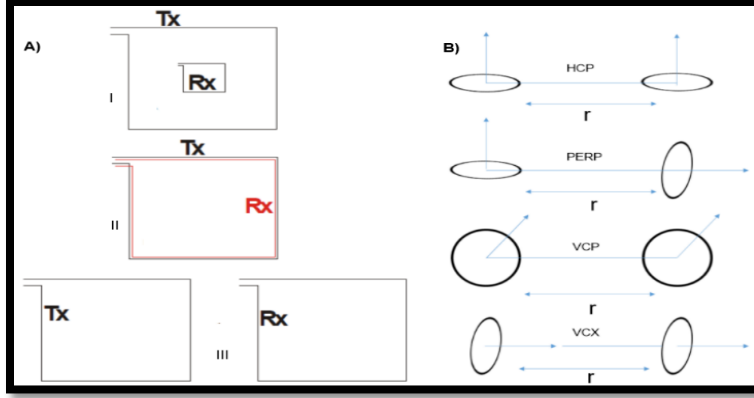


Figure 14. A) TDEM loops configuration, where Tx and Rx are the transmitter and the receiver, respectively; (I) – The transmitter and the receiver are in central loop; (II) – The transmitter and the receiver are coincident or the same; (III) – The transmitter and the receiver are laterally next to each other, (Adapted from Monteiro Santos, 2006). B) FDEM loops configuration; HCP – Horizontal coplanar; PERP – Perpendicular loop; VCP – Vertical coplanar; VCX – Vertical coaxial, (Adapted from Near-Surface Geophysics, Butler, 2005).

For the FDEM, the apparent resistivity for high frequencies can be calculated through the relationship:

$$p_a(w) = K \frac{\Delta V(w)}{I(w)} \quad (1.3.15)$$

Where, K is a constant that depends on the receiver and the transmitter utilized and the distance between them (similarly in sense to the geometric factor given in eq.1.3.7 for ERT), and can be calculated:

$$K = \frac{2\pi r^5}{9n_r S_r n_t S_t} \quad (1.3.16)$$

Where r is the distance between the transmitter and the receiver, $n_r S_r$ and $n_t S_t$ are the effective area of the receiver and the transmitter, respectively (Daniels, J. J., *et al.*, 1976).

For the TDEM, in late times, i.e. when the current is turned off, the apparent resistivity can be calculated:

$$\rho_a(t) = \left[\frac{\sqrt{\pi}}{20} \frac{\mu^{5/2} R^4}{t^{5/2} E(t)/I} \right]^{-2/3} \quad (1.3.17)$$

Where, $R = \frac{L}{\pi^{1/2}}$ is the effective radius of a single-turn square coil with a side L .

Usually, the instruments either FDEM or TDEM do not provide the apparent resistivity, some yield a measure of the output total field normalized by the input source, the impedance, or a measure of the amplitude and phase of the magnetic fields, like FDEM. While TDEM measure the electromotive force ($E(t)/I$) induced in ground in function of time, normalized by the intensity (I).

1.4. Characterization and geological context of the study area.

The selected areas (areas 1 and 2) have the same geological context and characteristics, so that, they will be explained together. These areas have been carefully chosen considering the information provides by geological maps. The profiles carried out in these areas were in potentially hazardous areas of contaminated water circulation.

For area 3, the information already presented and the suitability of the zone for construction, become this area in high interest to apply the geophysical methods.

1.4.1. Area 1 and 2 – Detection of contaminated groundwater.

1.4.1.1. Characterization.

The study area is characterized by its geological richness, especially in heavy metals such as copper, zinc, silver and lead being therefore used in their exploitation. Located in center-south Portugal, it's a massive sulfite deposit regionally belonging to the South Portuguese Zone (SPZ) and inserted into one of the largest reserves of volcanogenic sulfides in the world, the Iberian Pyrite Belt (Oliveira *et al.*, 2004).

The rock formations in the surrounding area of the study correspond to different types of shales and greywacke, allowing the circulation of water, since they have a high degree of fracture. Mining activity increases the risk for groundwater contamination and the existence of this type of geology increases the circulation through infiltrating in the subsoil.

Since there are large resistivity contrasts between fresh/contaminated groundwater and rocks, it is possible to identify lithological variations, tectonic structures and detect the presence of fractured zones with underground circulation. The profiles were set for this area in order to investigate the above mentioned processes.

1.4.1.2. Geological context.

The current state of geology began to be shaped in the Upper Devonian extending during the Carbonic (380-290 Ma) in the Paleozoic Era, giving rise to the Vulcan-Sedimentary Complex. This complex is divided into two temporally separated sequences: autochthonous sequence (Lower Vulcan-Sedimentary Complex [LVSC]) and allochthonous sequence (Upper Vulcan-Sedimentary Complex [UVSC]).

LVSC includes the Neves formation, which contains a black pyrite shale and thin-bedded siltstone as dominant lithologies. At the top of Neves formation, a shale layer with a few meters thick can be found, contain jasper and carbonate shales, ending the LVSC sequence (Oliveira *et al.*, 2004).

In the passage from LVSC to UVSC, at the beginning of the carboniferous, the Flysch Group is formed in a turbidite regime. This group encompasses the Mértola formation, made up of alternations of greywacke and dark gray shales approximately 3 km thick (Oliveira *et al.*, 2004).

The allochthones sequence (Upper Vulcan-Sedimentary Complex) was formed during the Middle and Upper Carboniferous, after Flysch group deposition. The sequence includes, from bottom to top, the Grandãos, Borra de Vinho, Godinho, Brancanes and Mértola Formations (Fig. 15).

The Grandãos formation comprises gray siliceous shale and black shale, generally enriched in organic matter. Borra de Vinho formation is a particular formation of UVSC which extends over the entire Pyrite Belt. It comprises purple and green shales, with a thickness varying from 10 to 40 m. The Godinho formation is composed of gray siliceous shales and tuffites. The layer thickness varies between 50 and 100 m (Oliveira *et al.*, 2004).

At the beginning of the Upper Carboniferous, Neves formation was settle. This was the beginning of turbidite sedimentation, leading to a new Mértola formation (Oliveira *et al.*, 2004).

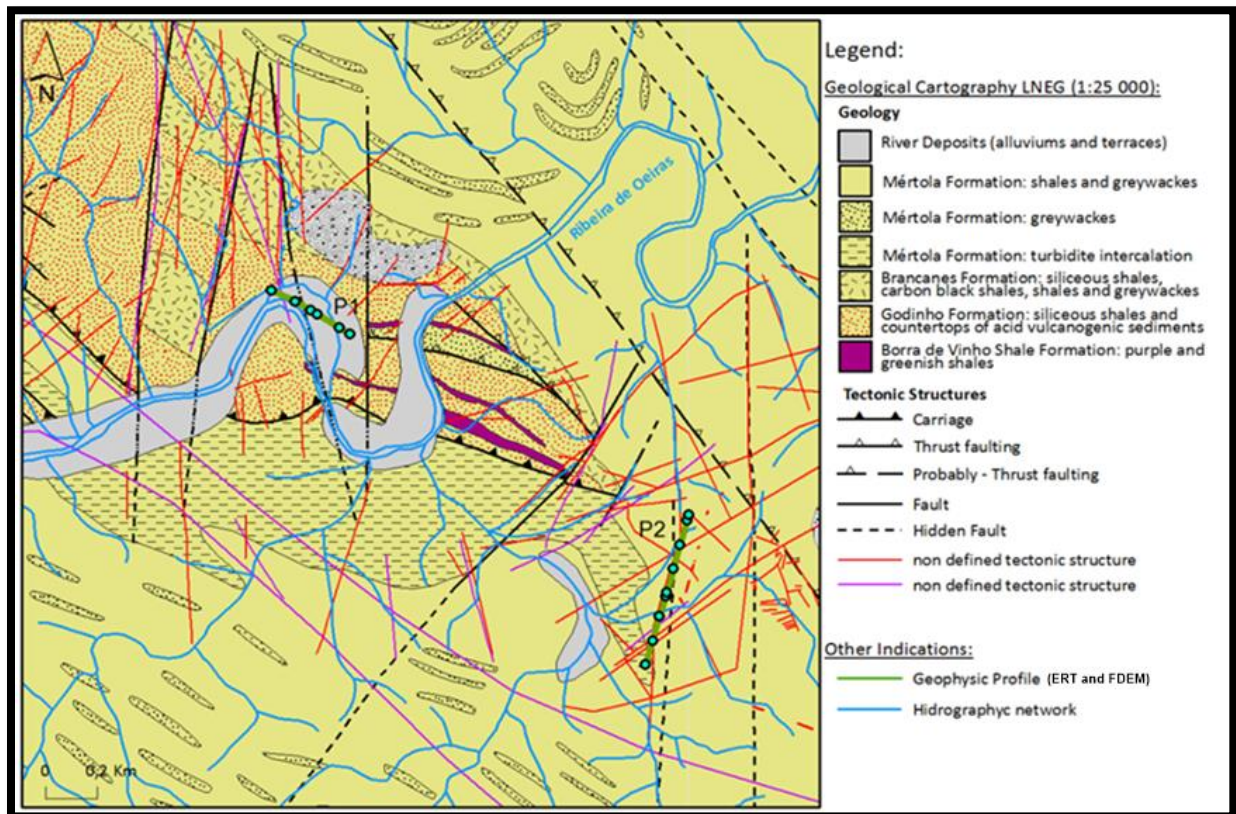


Figure 15. Location of the geophysical profiles (P1 and P2), and geological sketch of the study area [Modified from Geological Cartography – Laboratório Nacional da Energia e Geologia (LNEG)].

1.4.2. Area 3 - Engineering and geotechnical proposes.

1.4.2.1. Characterization.

This area was selected based on the possibility to be used in future construction and because some geotechnical studies have already been done. Hence, it is possible to further validate the existing geophysical profiles. The study area is in the Northern Lisbon Logistic Park (Parque Logístico Lisboa Norte - PLLN), in Castanheira do Ribatejo (Vila Franca de Xira).

It's located on the right bank of the Tejo river interconnected with highway roads and maritime infrastructures and it is seen, therefore, an optimal area for commercial activity. Due to the geological characteristics, the area needs a deep geotechnical exploration. It was previously used as a landfill, leading to a small layer of about 2-3 m with material of anthropogenic origin, construction debris.

1.4.2.2. Geological context.

The study area fits into the right bank of the lower sedimentary Tejo basin, extending along a floodplain, over 10 km (Fig. 16). It is a NE-SW depression, filled by an intercalation of sea and river debris flow.

The Tejo river floodplain is included in the domain of the Tejo Tertiary Basin, corresponding to an oriented depression according to NE-SW. It is limited to the W by Mesozoic units, and to the E by Cenozoic units with an extension of about 60 km. At the S, extends in a little contrasted way and continues into the Sado Tertiary Basin, (Zbyszewski and Torre de Assunção, 1965).

The Tejo Tertiary Basin is filled by sub-horizontal sediments and is limited by normal faults, except on the NW edge, where there is a thrust-fault contact.

Lithostratigraphic units represented in the study area, according to the Explanatory News Sheet 30-D Alenquer, Geological Services of Portugal, are represented by;

- ◆ Alluviums (Holocene), reaching a thickness of about 60 m. It is a fluvial-marine complex, consisting mainly of brown or dark gray sludge, sandy sludge, gray sands, alternations of sandy sludge and muddy sands, as well as muddy sands with gravel at the base;
- ◆ Deposits of river terraces (Plio-Pleistocene). Consisting of clays and conglomerates, clay sands and black clays; at the top, at least locally, there is a conglomerate with limestone elements;
- ◆ Some kilometers toward the N, are found formations from Pliocene (Ulme Formation), Miocene (Alcoentre Formation) and Paleogene (Benfica Formation). The reliefs to the W of the study area comprises limestones and pelites.

The geology presented in the study area has been confirmed by several prospecting studies (Lopes *et al.*, 2018), characterizing the different alluvial layers. Thus, from top to the base;

- ◆ Landfills, between 1.5 and 3.4 m thick. Consisting of sandy clays, sometimes with varying values of nature and size.
- ◆ Alluvial sediments, divided into 4 types from top to bottom: silt, silt sludge, silt clay, sandy gravel at the base. The thickness is approximately 46 m, including 8 to 10 m of corresponding gravel.
- ◆ Sandy clays and sparse conglomerate silt clay stones from Miocene, \approx 46 m in depth. Its thickness is between 3-6 m, according to the information from the drilling performed on the area.

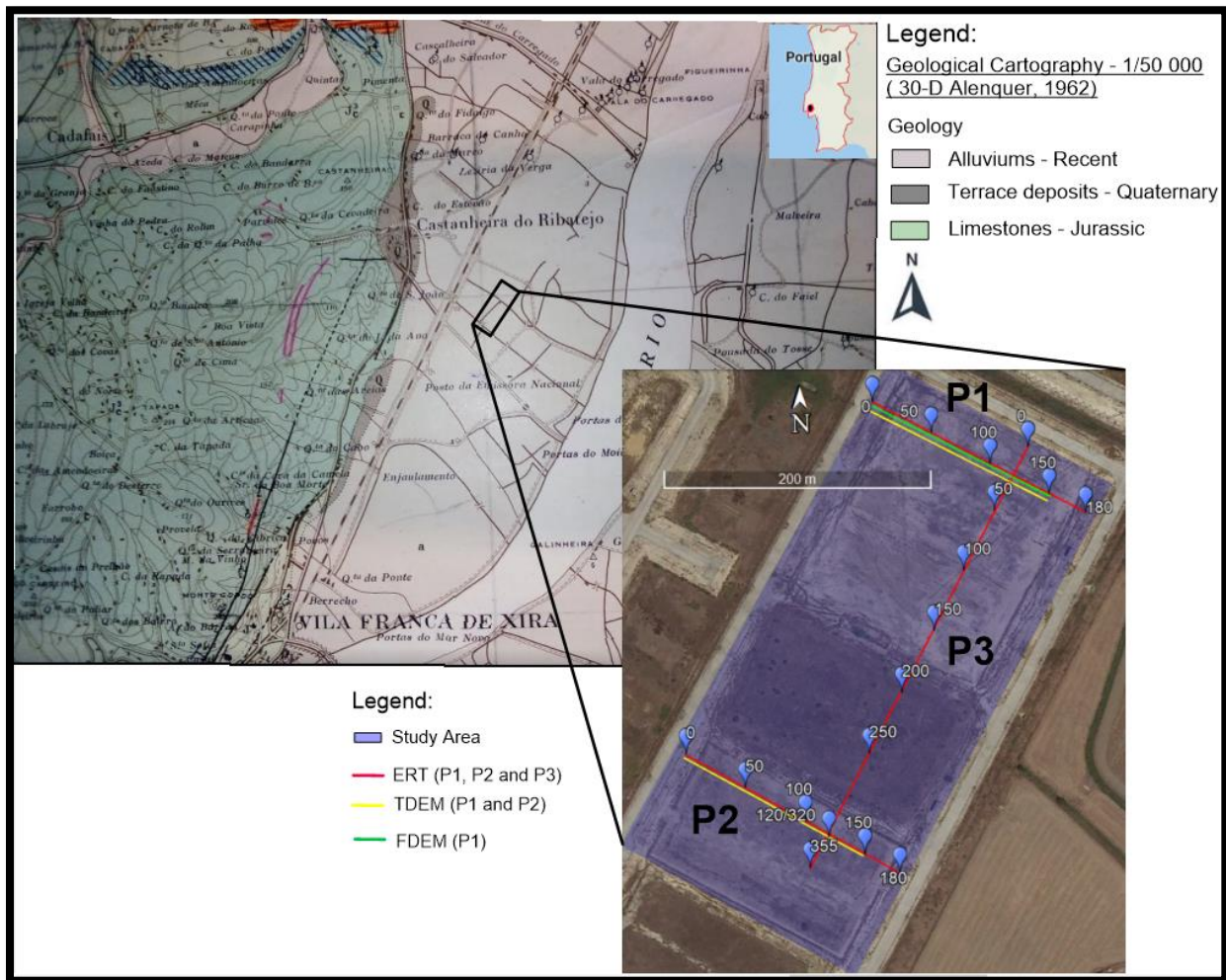


Figure 16. Location of the geophysical profiles inside the study area (below) and geological sketch of Area 3 (above).

1.5. Data Acquisition Methodology.

1.5.1. Electric Resistivity Tomography (ERT).

1.5.1.1. Equipment.

The Syscal Pro Switch (Fig. 17) was produced by IRIS Instruments. It comprises a maximum of 4 cables (90 m each) with 18 takeout, given rise a total of 72 outputs where electrodes are connected. The maximum electrode spacing is 5m and it is the spacing used in the profiles for all areas.

Three software were used: Electro Pro, which allows programming the sequence of measurement; Proxys II that allows the transfer data from Syscal to the computer; and RES2DINV for data processing.



Figure 17. Syscal Pro Switch instrument (left) with a 90m coil (right) and a connection cube for coils.

The necessary material for the acquisition is expressed next:

- ◆ Syscal Switch Pro unit;
- ◆ External battery (12 v; 60 amp);
- ◆ 72 electrodes;
- ◆ 4 cables with 90 m each;

- ◆ Hammer;
- ◆ Connections between electrodes and coils;
- ◆ 2 connection cubes.

And the software:

- ◆ Electro Pro;
- ◆ Proxys II;
- ◆ RES2DINV_{x32}.

1.5.1.2. Acquisition.

The acquisition of ERT profiles was carried out in the three areas mentioned in section 1.4. For Areas 1 and 2, the total length of the profiles was 355 m, while for Area 3 the length was 180 m for two of them (NW-SE) and 355 m (NE-SW) for the other. These differences in length will influence the depth reached, but for the purposes of the geotechnical issues, 180 m length was enough.

Acquisition consists of three steps:

1. Create a sequence of readings.

Before starting the acquisition, it is necessary to define the array and order of measurements, thus enabling the readings to be automatized and no operator intervention required.

A type of measurement was then created. In the present case a straight line with an electrode spacing of 5m. As it was mention in the last sections, there are different types of array. For the present work, it was used the Wenner-Schlumberger configuration shown in Fig. 18. The maximum theoretical depth of investigation was 68 m. The data acquisition sequence, for the first and second measures, is illustrated in Fig. 19.

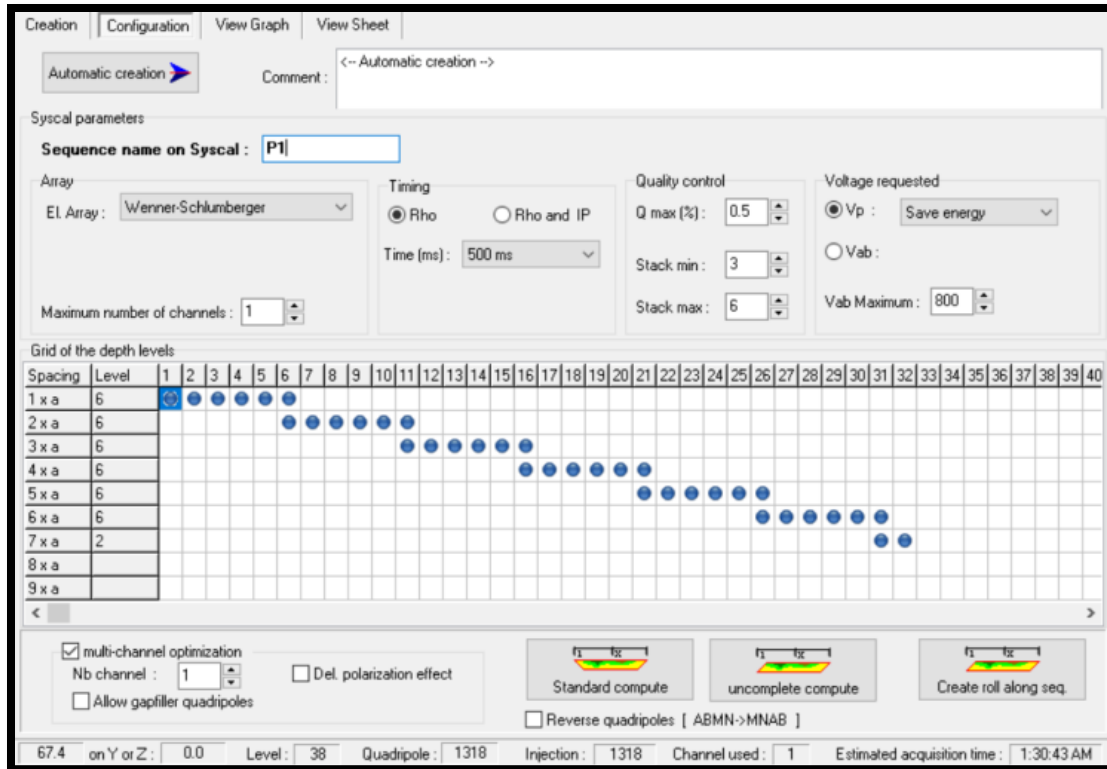


Figure 18. Creation and configuration of the reading sequence, Electro Pro Software.

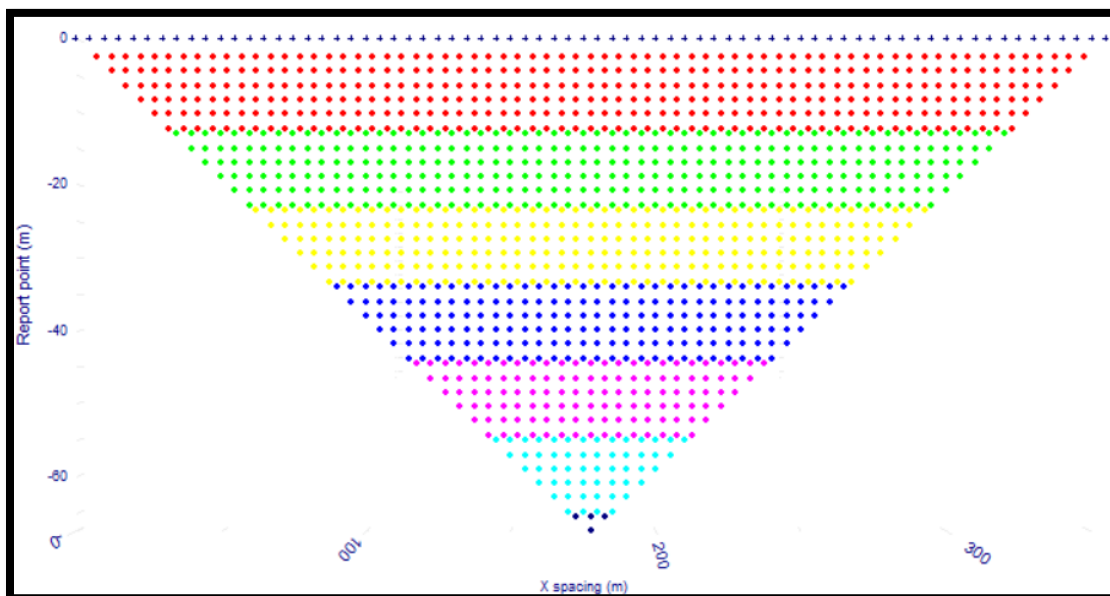


Figure 19. Graph of the readings. Each dot represents a data point and the different colors represent the levels, which are defined through the space between MN electrodes, Electro Pro Software.

After the straight-line creation, there are several quality control parameters that have to be fulfilled. The parameter Q gives us the maximum allowable error percentage (Q_{max}) which was defined as 0.5% and a number of measures made for each reading ($Stack_{min}$, $Stack_{max}$), set as 3 and 6 respectively. The time between each injection was set at 500ms.

The sequence is then uploaded to the Syscal Switch Pro and saved.

2. *Field acquisition.*

For each profile, the four cables are extended in a straight line, with the help of a GPS – is always needs two or more persons for not make tension on the cable. Then, the electrodes are placed in the ground at 5m distance to each other and aligned with the coil. Finally, the connections between the coil/electrode are placed, as it is shown in Figure 20.

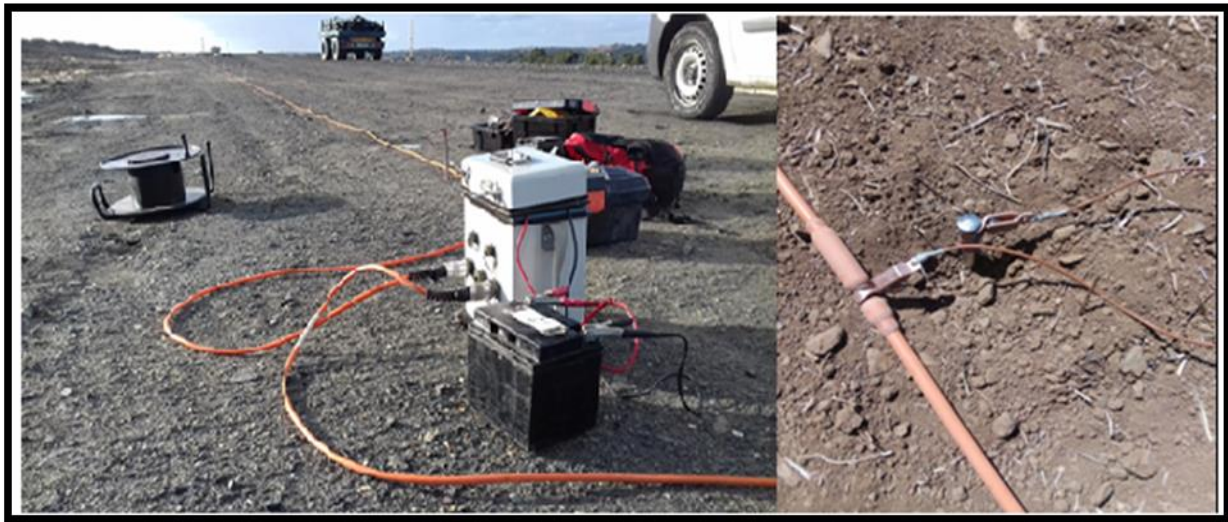


Figure 20. Extended coil with the main Unit (left) and installation of the electrodes and connections (right).

After extending the profile line, its necessary check if the electrode/ground contact resistances are good (low contact resistance). For a good quality of the data, the resistance values should be lower than 10 KOhm.m. In the electrodes where the resistance contact is poor, it is necessary to check or replace the connection, even adding some saltwater to improve the resistance contact.

The readings start with electrode A fixed and the MN potential electrodes kept together while the electrode B, jointly with MN are spaced 10m from A, for each reading (Fig. 21).

When the reading reaches the second level (green level), the MN are spaced 10 m between them and kept the same distance until reaches the other level (yellow), which happens when B reaches the end of the line, when the space between them will be 10 m, in every level the distance between MN will rise 5m, this keeps going until the end of the line. When the B electrode reaches the end of the line the process restart from the beginning, now with the electrode A be placed 5m from its original position. For a profile with 355 m, the acquisition time was one hour and a half.

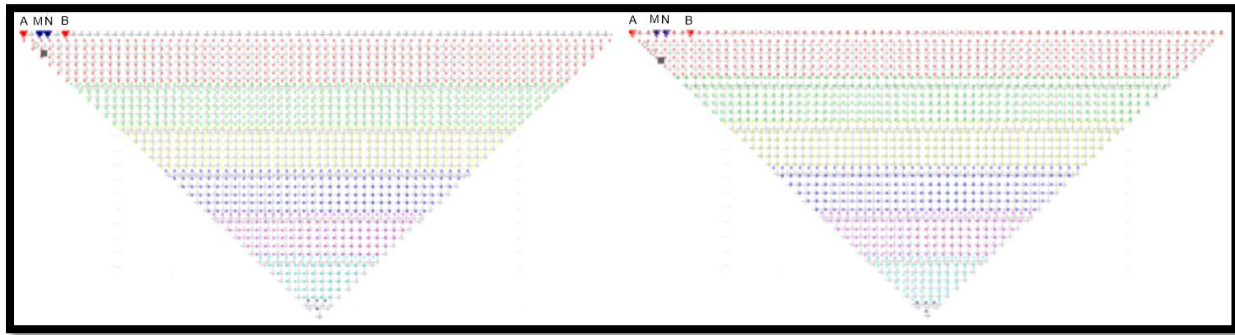


Figure 21. Left – Second reading; Right – Third reading. AB – Current electrodes; MN – Potential electrodes; Black dot – Reading. The colors represent measurement levels.

3. Transfer the data.

Data transfer is made it by a USB cable connected to the main unit (Syscal) and to the computer. The software used for this was Proxys II. This software allows it to export the data file in various formats for later calculations. In this case, the data file was export and saved for be used in RES2DINV, (Fig. 22).

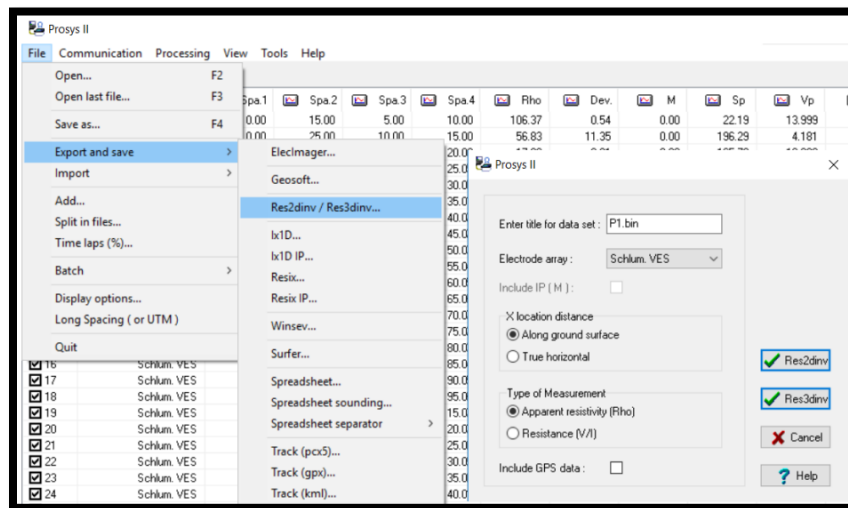


Figure 22. Data transfer using the Proxys II software.

1.5.2. Time-Domain Electromagnetic (TDEM)

In this method, the cables were placed directly on a ground surface. Compared to resistive methods, they are less work time-consuming. However, their resolution is slightly lower than direct current resistivity methods for small structures, especially for the shallower features.

1.5.2.1. Equipment.

For the TDEM acquisition, the equipment used was the TEM-FAST 48 HPC, which is a portable equipment developed by AEMR Ltd. Company. All together the TDEM device consists of: the main unit, a black box with the receiver, the transmitter, and other components incorporated; an IPaQ Pc, with TEM-FAST 48 HPC program incorporated and a coil with 50m length, Figure 23.



Figure 23. TDEM acquisition device, (adapted from www.aerm.net).

Summarizing the necessary material for the acquisition:

- ◆ IPaQ PC;
- ◆ Connection cables for - External battery with a 24v Power, main unit with single-loop coil, main unit with IPaQ Pc);
- ◆ Two coils with 100 m length;
- ◆ Main Unit (Receiver and Transmitter).

And the software:

- ◆ TEM-FAST 48 HPC;
- ◆ TEM-RES v.7.

1.5.2.2. Acquisition.

The TDEM profiles were performed only for Area 3. Three profiles were carried. Two of them with loops of 25 m, 10 m spaced along a profile of 150 m, which gives 15 soundings per profile and a total of 30 soundings. The third one was carried out for a 50 x 50 m loop consisting of 20 m spaced soundings along a 150 m, which gives 7 soundings in total (Fig. 16).

The loop configuration adopted was a single-loop. It's more efficiently in the field than other arrays, and it allows it to measure the variations of the magnetic flux through the loop.

Moreover, the decay of the current depends on the size of the coils, thus, although with a 25 m loop reached the objective, the use of a 50 m loop was used to confirm in depth the results.

For the acquisition, as in ERT, the process will be divided into three steps. First, there are a few parameters that must be defined in TEM-FAST 48 HPC; secondly, data acquisition and finally, transfer and correct the data.

1. Set the Parameters for the reading.

Before starts the readings, it is necessary to define some parameters that will influence the depth reached, noise and quality. The parameters chosen are present in Figure 24 and described next:

- ◆ TR and REC –Transmitter and receiver loops dimension.
- ◆ I – Current intensity (A). For an input current of 12 V, for the 25 x 25 m loop, 1-4 A was used; for the 50m x 50m the input current was 24 V and the current intensity was 1-4 A.
- ◆ Time – A range of measurements (μs). For the 25 x 25 m loop case, the time of the measurement reached $7652.2 \mu\text{s} = 8$. For the 50 x 50 m loop, the time of the measurement reached $3826.1 \mu\text{s} = 7$.
- ◆ Stack – It's a parameter of signal digital stacking.

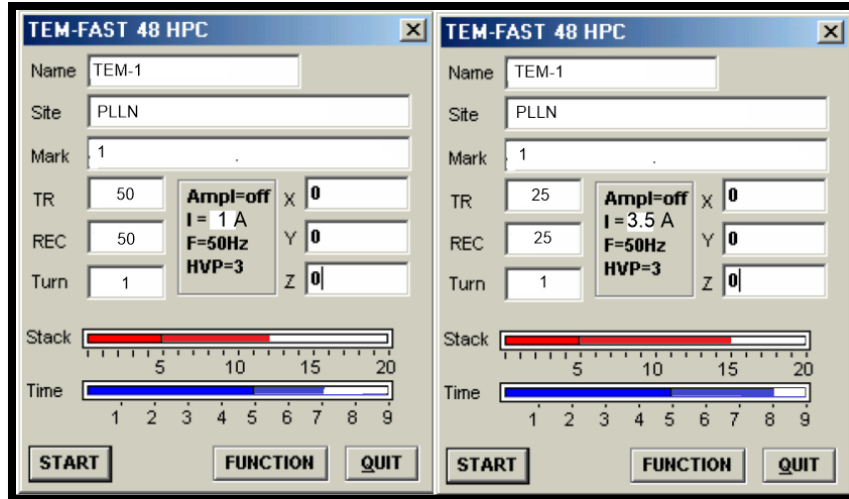


Figure 24. TEM-FAST 48 HPC parameters; Left – For 50m x 50m loops; Right – 25m x25 m.

2. *Take the readings, check data quality and transfer to Pc.*

After the parameters set up, the cable is extended in a square and the main device is connected to the battery, cable, and IPaQ (Fig. 25).

When measuring ends, the data are plotted on the screen and can be visualized in two parameters in function of time; the resistivity (Ohm.m) and the impedance (V/A). This allows it to verify the quality of the data in the field and proceed to another measure if the curves of these parameters have an anomaly.

Finally, the data is transferred to a PC through an SD that is contained in the iPaQ. The data is converted in a compatible format for the processing program TEM-RES.



Figure 25. All components of the TEM-FAST connected to the main unit.

1.5.3. Frequency-Domain Electromagnetic (FDEM).

1.5.3.1. Equipment.

The equipment used was the FDEM-8, which is an affordable frequency domain equipment produced by Des Barlow (Fig. 26). It consists of a transmitter and receiver, connected by a synchronization cable and it can acquire readings for eight frequencies (37 to 4800Hz) in each station of measurement. It also contains two coils, connected to receiver and transmitter with dimensions 760 x 40 mm. The display results are in Amplitude (mV) or in-phase ($^{\circ}$).



Figure 26. FDEM-8 (Des Barlow) – Coils (red), transmitter (right) and receiver (left).

The necessary material for the acquisition is expressed next:

- ◆ Two coils;
- ◆ Connection cables for - Receiver/Transmitter and connection with the coils, respectively;
- ◆ Receiver and a Transmitter;
- ◆ Measuring tape.

Software:

- ◆ PCFDEM

1.5.3.2. Acquisition.

The FDEM profiles were performed on the three Areas. The profile for Area 1 consists of 10 m spacing sounding along 200 m, with the space between the centers of the coils fixed at 20 m (Fig.15). For Area 2, the profile consists of 10 m sounding along 400 m, with the space between the centers of the coils fixed at 20 m, (Fig. 15). Finally, for the third profile 10 m space sounding was collected along 150m, with the space between the centers of the coils fixed at 20 m (Fig. 16).

The coil configuration used was a horizontal coplanar loop (HCP), (Fig. 14-B). It generates a vertical magnetic dipole (VMD). It was the configuration adopted due to the dipole position because compared to the vertical coplanar loop (VCP), where the magnetic dipole is horizontal (HMD), it reaches higher depths. However, for shallow depths, the resolution is not as good as the HMD.

The acquisition took place in three phases: set measuring parameters, data acquisition, and data transfer.

1. *Set the parameters for the reading.*

It is necessary to set certain parameters before the readings. In this case, the parameters correspond to the geometry of the acquisition. The setup menu is present in the receiver screen, (Fig.27). Thus, it's set the frequencies that will be displayed on the screen during the acquisition. However, all eight frequencies will be saved. The spacing is the distance between the two coils and was set to 10m for Area 1 and 20m for Areas 2 and 3.

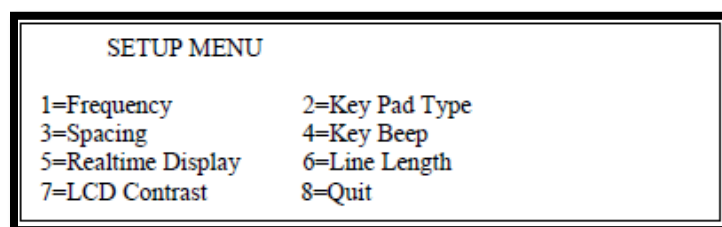


Figure 27. FDEM-8 setup menu.

2. Assemble the line and take readings.

In order to be rigorous with the spacing of the data acquisition, a measuring tape was placed on the ground defining the position of the measurements. Later, the coils were placed on the line with respective spacing and the receiver and transmitter cables were connected to the coils (Fig. 28).



Figure 28. FDEM-8 sounding assembled.

Data acquisition takes approximately 30 seconds for each measurement. After that, the coils are moved to the next position and the readings continue.

3. Transfer data to Pc.

Data transfer was performed using PCFDEM software. At the end of the acquisition, the field unit is connected to the computer and the *transfer data from the Receiver* option is selected. Data can be converted to various formats for later use in different software (Fig. 29).

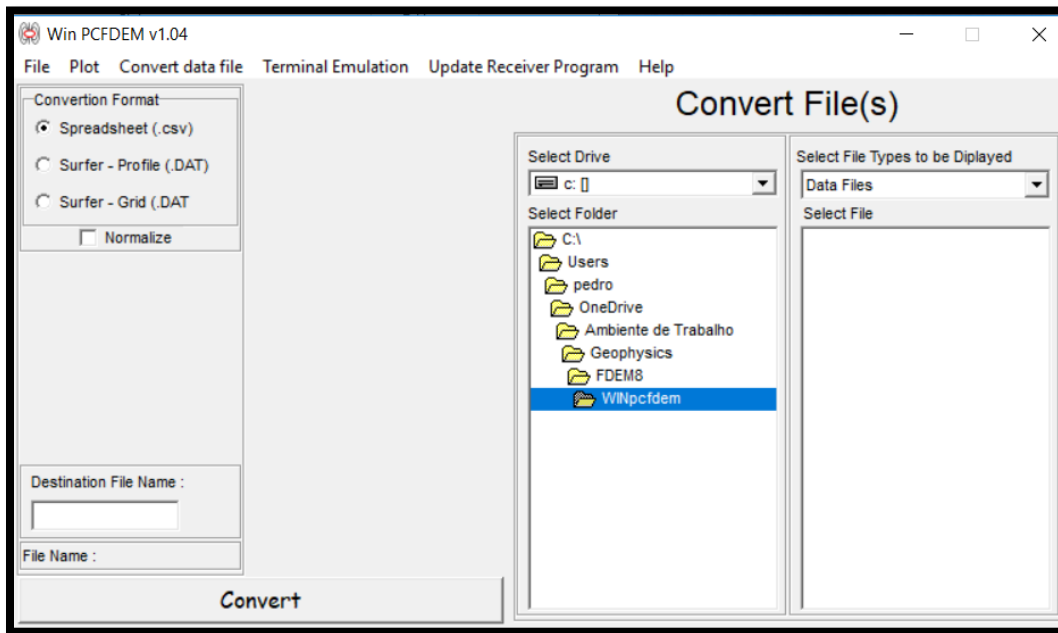


Figure 29. Different formats of data conversion in PCFDEM software.

It's important to mention the normalization of the data. In this case, the data was normalized by the intensity of the current I (mA) as is shown in table 1, for the different frequencies.

Table 1. Output Current for the different frequencies in FDEM-8.

FREQUENCY	OUTPUT CURRENT	OUTPUT Atm^2
4800	143 mA	3.24
2400	223 mA	5.06
1200	413 mA	9.37
600	752 mA	8.91
300	1203 mA	27.29
150	1529 mA	34.68
75	1639 mA	37.18
37	1577 mA	35.77

1.6. Data Processing.

1.6.1. ERT – RES2DINV program.

Prior to the inversion, the bad data points are discarded as shown in Figure 30. The main purpose of this option is to eliminate the data points that have anomalous values. This can happen due to soil/electrode contact resistances or relays malfunction in one of the electrodes.

After the correction of anomalous data points, the initial model is defined and the inversion process starts. For the initial model, the following parameters were selected: the horizontal mesh, the one which gave us the best result was a *4 node mesh* because we have high resistivity contrasts; the vertical mesh size, was defined as the *normal mesh* and, for the direct problem, the type of method adopted was the *finite-difference method*. These parameters were the same for all ERT profiles.

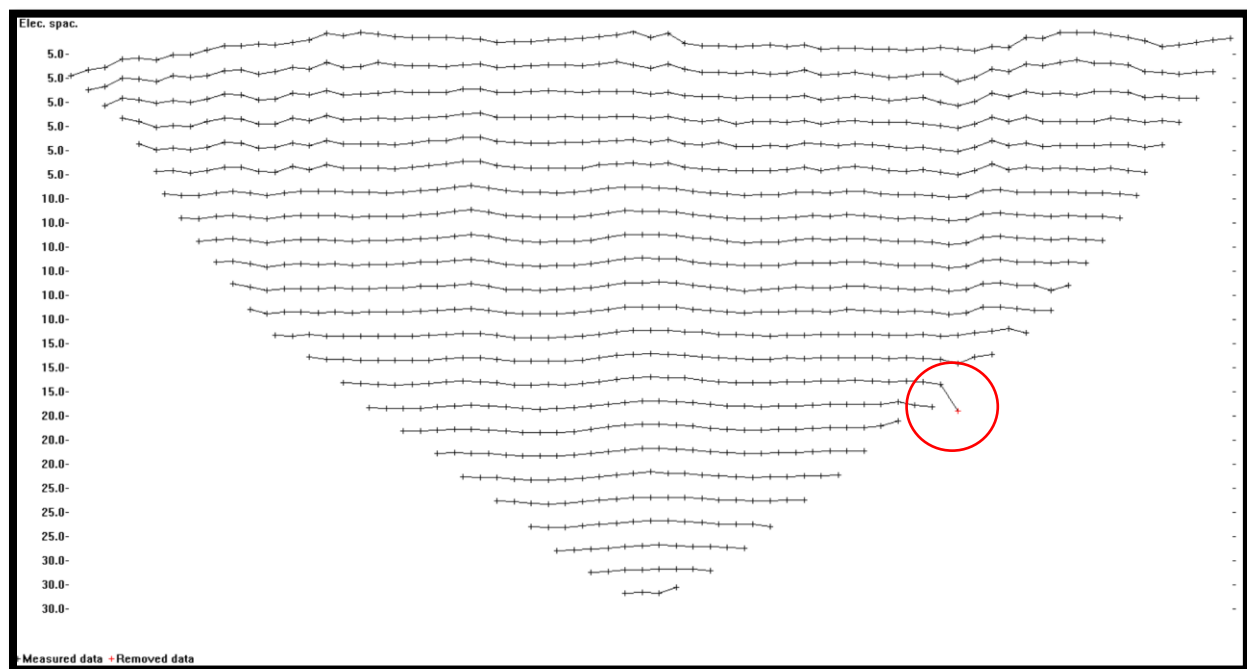


Figure 30. Example of the Profile in Area 1 – Correction of the bad data points in RES2DINV software, for the profile in Area 1.

The RES2DINV is a program that uses the *least-square inversion* to optimize the data model response, which means that will be attempt to minimize the square of a difference between the measured and the

calculated apparent resistivity. However, for the data that contains ‘outliers’ data points, this method is less satisfactory.

These ‘outliers’ will influence the inversion result. To reduce its effect, an L1 norm method (robust constraint) was selected, where the absolute difference between the measured and calculated apparent resistivity values is minimized.

The result for the measured and calculated apparent resistivity and the inverse model resistivity section is present in Figure 31.

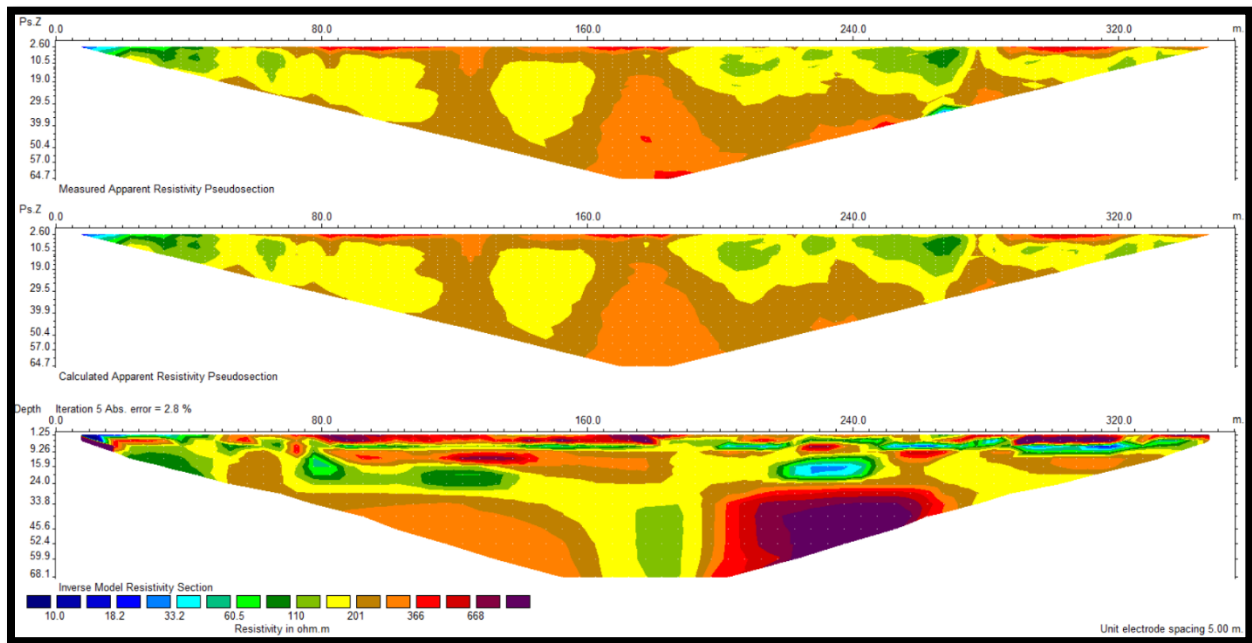


Figure 31. Example of the Profile in Area 1 – From top to bottom; measured apparent resistivity; calculated apparent resistivity and the inverse model.

1.6.2. TDEM – TEM-RESEARCHER program.

For the data processing, the program used was the TEM-RES which is intended for modeling and inversion of TDEM sounding data. First, the input field data is open in the program and can be represented in various formats; RES (t) - apparent resistivity in function of time ($\rho_a(t)$); E (t)/I – Electromotive force (EMF) in the receiving coil normalized at current I; and t*E (t)/I – which is a product between the time and the EMF.

After that, quality control of the data must be done. Two tools are used: the edit field data and smooth field data. The edit is used for ‘outliers’ correction, and *smoothing* is selected after that (Fig. 32).

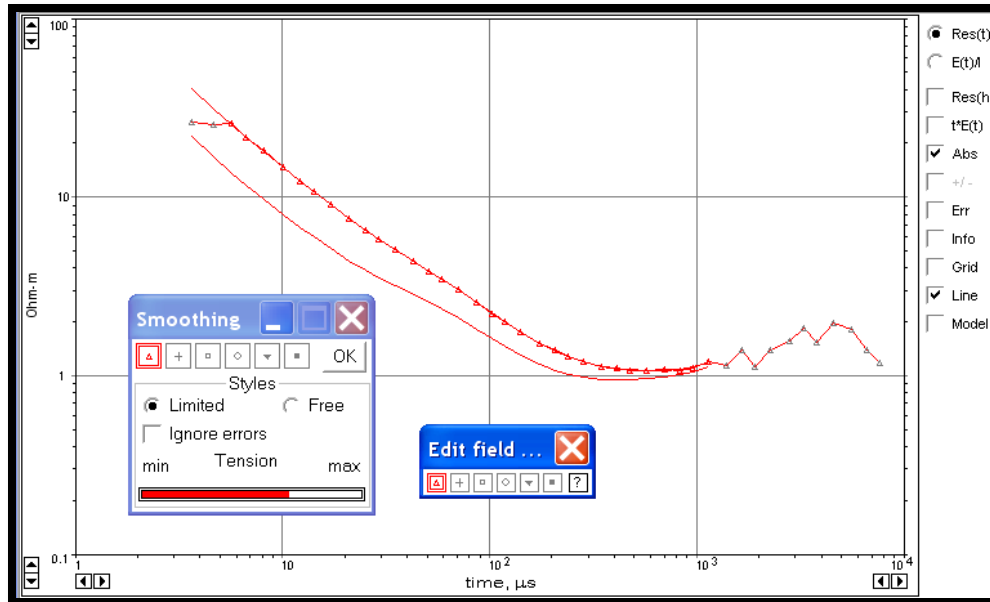


Figure 32. Example of one sounding of the Profile in Area 3 – Edit and smoothing field data in TEM-RES.

Then, the initial model can be constructed in two ways: based on apparent resistivity $\rho(t)$, or on the basis of apparent conductance $S(h)$.

For the present work, the initial model was defined with 3-4 layers, depending on the data of sounding, and based on the apparent resistivity. Finally, the TEM-RES inversion process is carried out, adjusting layer thickness and resistivity values in order to have minimal data misfit.

For a good model fit the average misfit must be lower than 5%. In the present work, the % of misfit was between 1-4%. The initial and the inverse models are present in Figure 33 for one sounding.

After inversion of all TEM soundings, the results are gathered and plotted in a cross-section. The cross-section was cut at 30 m because, in a presence of a very conductive layer, the wave energy stokes into that layer and thus the vertical resolution it is not so clear (Fig. 34).

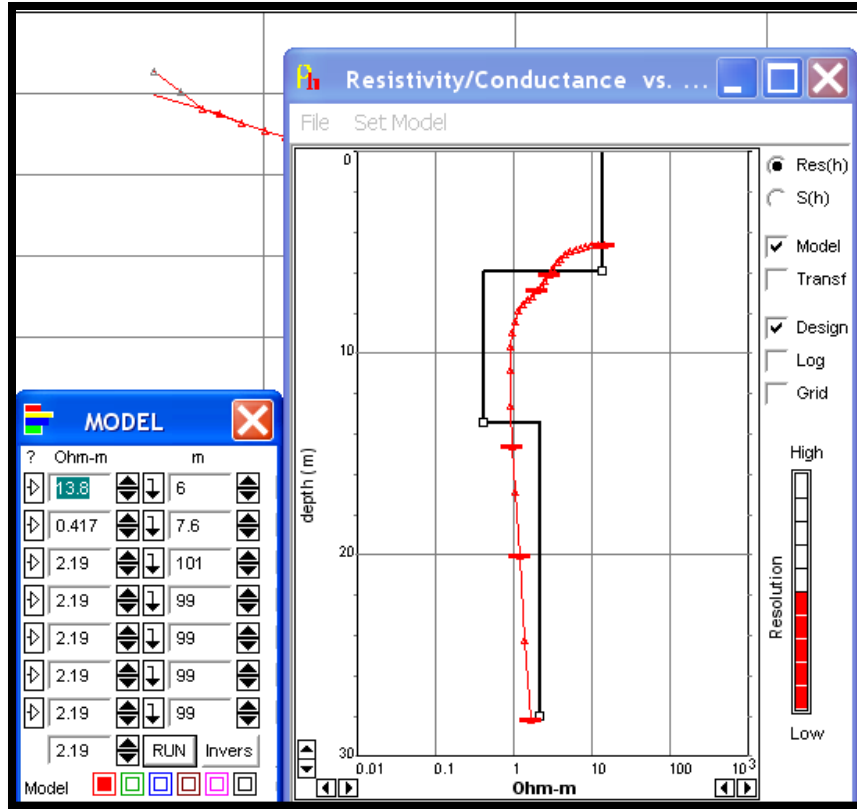


Figure 33. Example of one sounding forward model creation in TEM-RES – A model with 3 layers.

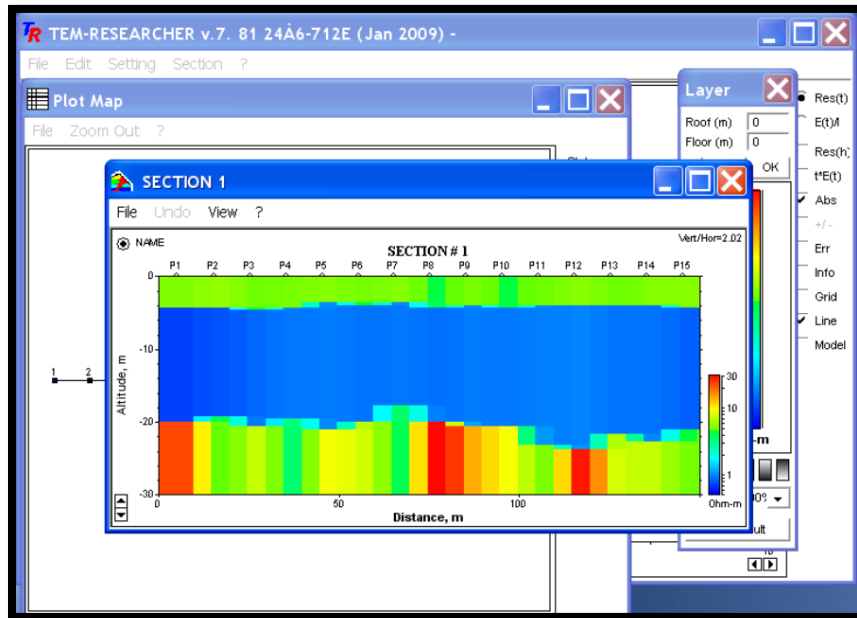


Figure 34. Cross-section creation in TEM-RES software.

1.7. Results.

1.7.1. Location of contaminated waters.

Profile 1.

The ERT profile was carried out over a possible contaminated groundwater area. It was expected little areas of contamination and possible appearance of fault zones. The FDEM profile has 200 m length matching from the 80 m with the position of the ERT profile with 355 m length.

The results of P1 are represented in Figure 35 and are described below:

- ◆ The profile developed over a water stream that covers the Godinho formation presented an unsaturated layer in the first depth meters of the profile (0-5 m depth) and extended along the 355m, with resistivities of 300-600 ohm.m. This layer is well recognized throughout the FDEM profile, however, with lower resistivity values. At the beginning of the profile exists a very low resistivity area (C1) concerning to the shallow contaminated area coming from the mining reservoirs.
- ◆ Under this resistive layer, there is a thin layer (1-2 m) with low resistivity of about 30-50 ohm.m corresponding to fresh groundwater circulation.
- ◆ Below, the resistivity reaches higher values of 300-400 ohm.m corresponding to the unsaturated area. This layer is interrupted at 220-250 lengths with an area of low resistivity values of 20-30 ohm.m that is interpreted as a contaminated groundwater zone.
- ◆ In terms of tectonic structures, two faults were detected, at 45 m and at 210/120 m (ERT / FDEM). These faults allow the groundwater circulation. As identified in Figure. 35, the fault zone is filled with sediments with relatively low resistivity (60-100 ohm.m), without contaminated water. Hence, it corresponds to saturated rocks with fresh water. The water recharge of these zones is produced by the faults located on the meters 45 and 200 lengths.
- ◆ Regarding possible groundwater contamination by sulfide, two potential zones were detected, C1 and C2. C1 is the cross between the profile and the contaminated water circulation ducts (low resistive values of 10 ohm.m), due to discharges made from the mineral separation processes. The C2, between 210-245 m in the ERT and 140-175 m in the FDEM, represents a possible water flow in the NE-SW direction. There are no signals of more contamination around this area, consequently, the recharging presupposes to follow the mentioned direction, derived from the mining reservoirs.

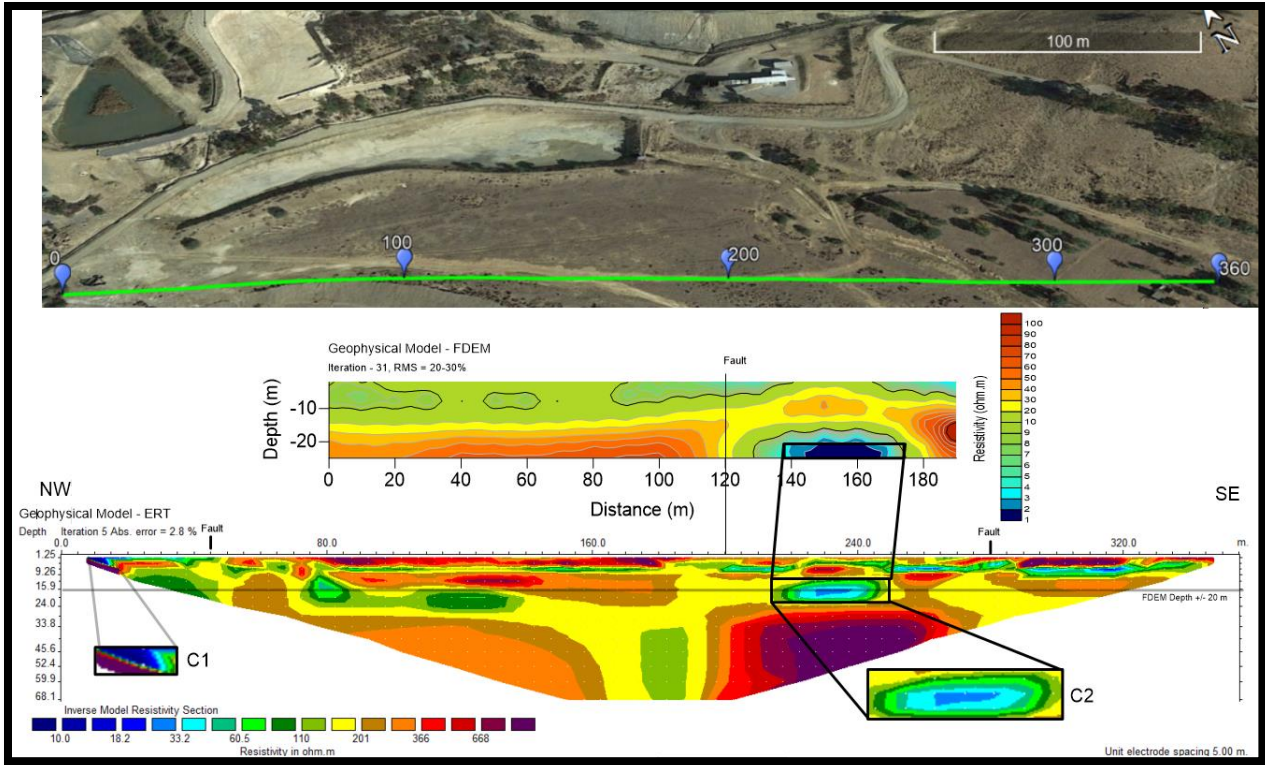


Figure 35. Results from Profile 1. ERT (bottom), FDEM (Top). Location of contaminated groundwater (C1-C2). The FDEM depth is represented in the ERT profile by the grey line.

Profile 2.

The ERT profile was made to the east of P1, located next to a non-contaminated water reservoir, so few contamination of water flow is expected. The FDEM profile has a 90 m shift from the ERT Profile.

The results of this profile are showed in Figure 36 and are described below:

- ◆ It presents an irregularity in the layers, characterized by the high existing fracturing. However, it is possible to check surface areas with high resistivity (> 400 ohm.m) about 12 m thick between 240-320 m and 400-530 m in the ERT profile and confirmed in the FDEM profile. In depth, it is interspersed by zones of low and high resistivities along the profile.
- ◆ In tectonic terms, five potential faults were found; at meters 110, 240, 335, 390 and 530 length from the ERT profile, four of them are well marked in the FDEM result. These five faults are the main factor behind the variability of resistivity values present in this zone, allowing the circulation of water between resistive massifs, leading to great resistivity contrasts. It is possible to detect a deep decrease in the resistivity value in these same zones (Figure 36, *'freshwater circulation'*), ranging from 18-70 ohm.m. Some of them belong to possible contaminated zones (C1 and C2) and others to freshwater circulation or saturation.

- ◆ C1 indicates a contaminated circulation zone (≈ 18 ohm.m), probably coming from the mining reservoir situated E. However, being close to fault zones, this C1 could be originated from surface recharges and accumulate in depth.
- ◆ C2 coincides with a fault, with the same origin as C1, but has relatively higher resistivity values (25 ohm.m).

Between 335 and 390 m length, and 50 m depth exists a low resistivity area (≈ 40 ohm.m) that coincides with the position of the water channel at the surface

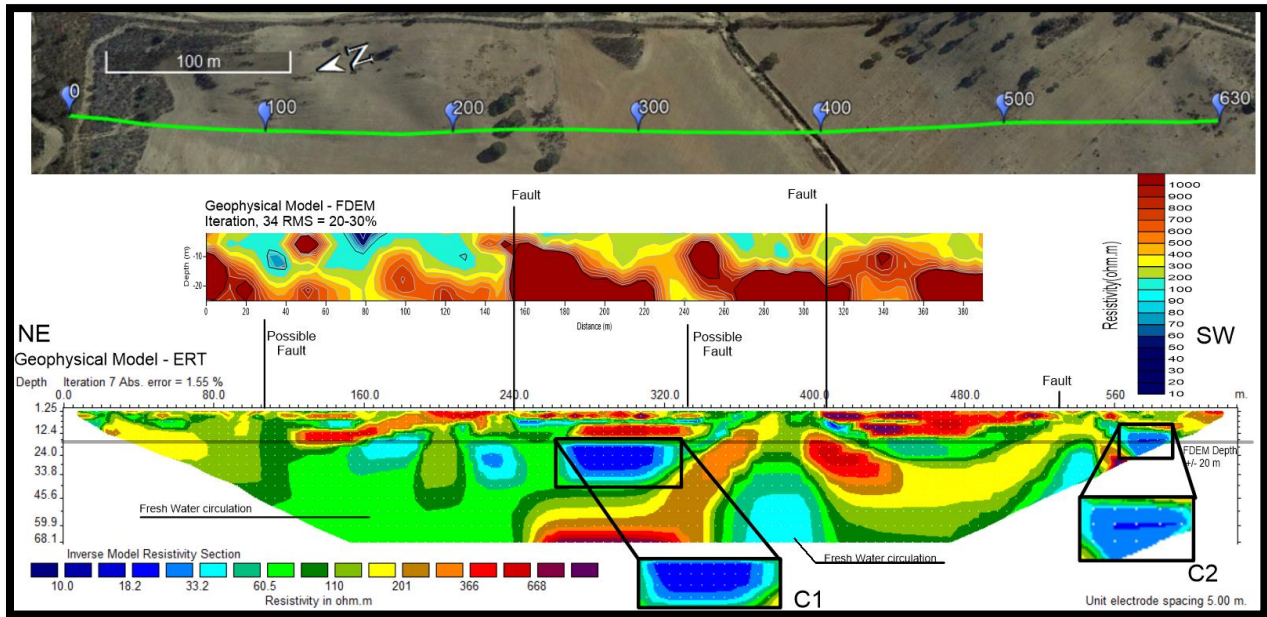


Figure 36. Results from Profile 2. ERT (bottom), FDEM (Top). Location of contaminated groundwater (C1-C2). The FDEM depth is represented in the ERT profile by the grey line.

1.7.2. Engineering and geotechnical purposes.

Profile 1.

This profile was acquired over an alluvial zone with the shallowest meters filled by landfill deposits. In both profiles (TDEM, FDEM, and ERT), three layers are well marked by the resistivity contrasts.

The results of this profile are expressed in Figure 37 and will be described below;

- ◆ The shallowest layer (L1), about 5 m thick, has high resistivity (100-300 ohm.m in ERT), corresponding to the mentioned landfill deposits. In TDEM the low resolution at the first meters is due to the loop size, and it does not allow to correctly detect the resistivity values. However, they are relatively higher than the adjacent layer.
- ◆ From 5 m downwards, a layer of about 15-17 m thick with very low resistivity (1-5 ohm.m) appears along the entire profile, being well referenced in both ERT and TDEM. This layer, due to its low resistivity, is related to the presence of clays in depth. As noted in section 1.2.4.3, clay has a very peculiar effect on measurement results, decreasing the resistivity.
- ◆ At the bottom of the profile appears a more solid layer compared to the previous one, with resistivity values of 20-30 ohm.m. This layer is well defined in TDEM and FDEM with values like those of ERT. The thickness of the layer is not determined, however, it is visible from Figure 37 the increasing appearance of depth resistivity (L2), which may be the beginning of the bedrock (approximately 30 m).

Profile 2.

This profile was measured 300 m toward the south of profile 1 in order to relate them, with the same direction and lengths. As in P1, the horizontal arrangement of the material is visible, composed of three well-defined layers by both ERT and TDEM.

The results of this profile are shown in Figure 38 and described below:

- ◆ The shallower layer of 5 m thick has a resistivity of 25-50 ohm.m that extends throughout the profiles. However, as in the previous profile, the TDEM profile does not record the resistivity at the first meters.
- ◆ From 5 m depth, the resistivity drops to values in the order of 1-5 ohm.m (L1). This layer has an irregular thickness up to 80 m length in the ERT profile, thereafter it has a thickness of about 10-15m. This layer is well marked in TDEM, with resistivity values equal to ERT (1 ohm.m).

- ◆ At the bottom of the profiles, a more resistive layer (L2) appears, with resistivities ranging from 10 to 30 ohm.m. It can be observed in the TDEM profile, a gradual advance of resistivity values from 80 m (20 m depth), validating the ERT results.

This profile has reached a depth of investigation of ≈ 30 m.

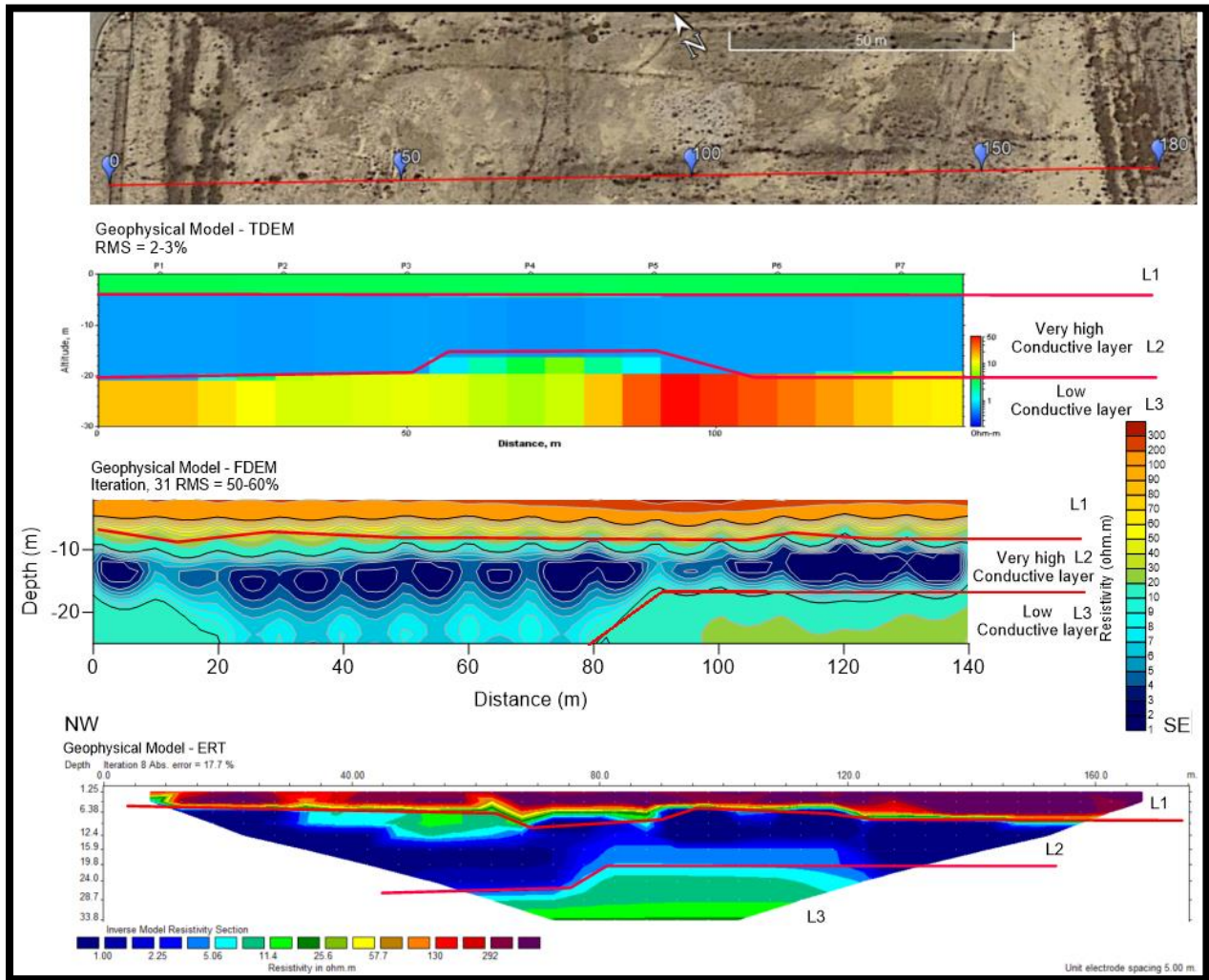


Figure 37. Results from Profile 1. ERT (bottom), FDEM (Middle) and TDEM (Top). The layers are represented by red lines (L1, L2, and L3). Engineering and geotechnical purposes.

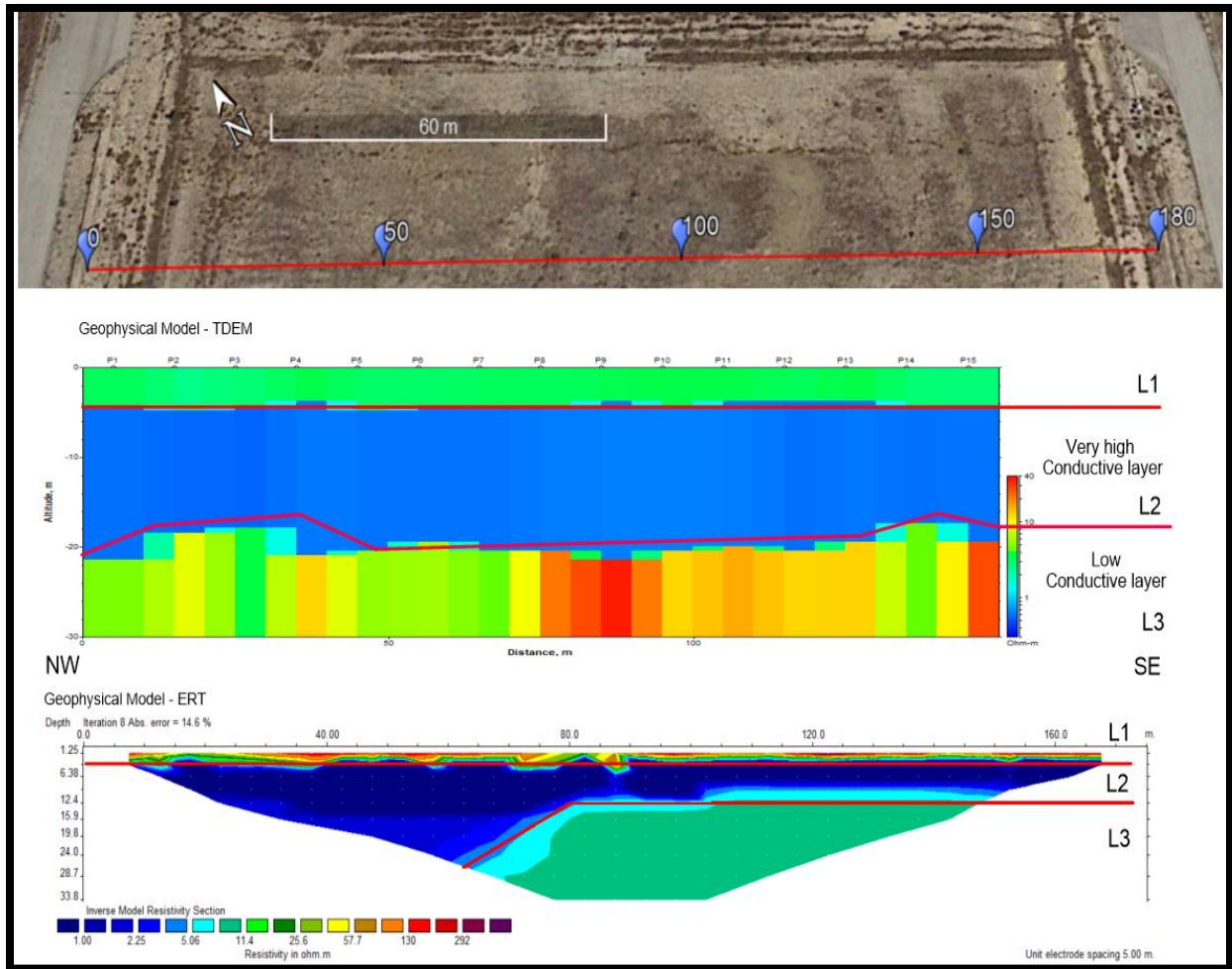


Figure 38. Results from Profile 2. ERT (bottom) and TDEM (Top). The layers are represented by red lines (L1, L2, and L3). Engineering and geotechnical purposes.

Profile 3.

This profile reaches greater depths of investigation and it has a different orientation than the previous one in order to have a NE-SW view of the whole area (see Fig. 16). It was performed perpendicular to profiles 1 and 2, crossing them at 130 m length.

It has the same surface structure and resistivity values than the previous profiles, achieving a depth of investigation of 68 m with a length of 355 m.

The results of this profile are shown in Figure 39 and are described below;

- ◆ It has a first layer with a resistivity of 100-200 ohm.m and approximately 5 m thick up to 195 m length in the profile, and then significantly increases in thickness to 15 m. This more resistive surface layer, highlighted in all profiles, may have anthropic origin as mentioned above.

- ◆ Like the other profiles, from 5 m downwards, a layer with very low resistivity values (L2), 1 ohm.m, has a constant thickness up to 195 m, spreading from there. These values may indicate the presence of clay.
- ◆ Below, there is a more resistive area in relation to the previous layer (indicated as R1 and R2 in Fig. 39). They present resistivities of 10-30 ohm, matching with the other profiles. Embedding in this layer, between 195-270 m lengths, there is a very low resistivity layer of 1 ohm.m corresponding to the presence of clay, as in the L2. This change in resistivity suggests the presence of two faults at both sides of the low resistivity area. R1 and R2 may represent the bedrock, and the area in the middle the fractured bedrock with clays into.

The results of this profile were satisfactory, allowing to identify zones of possible bedrock, as well as possible zones of clay material, being zones of low mechanical robustness with risk of subsidence when applied too much compression.

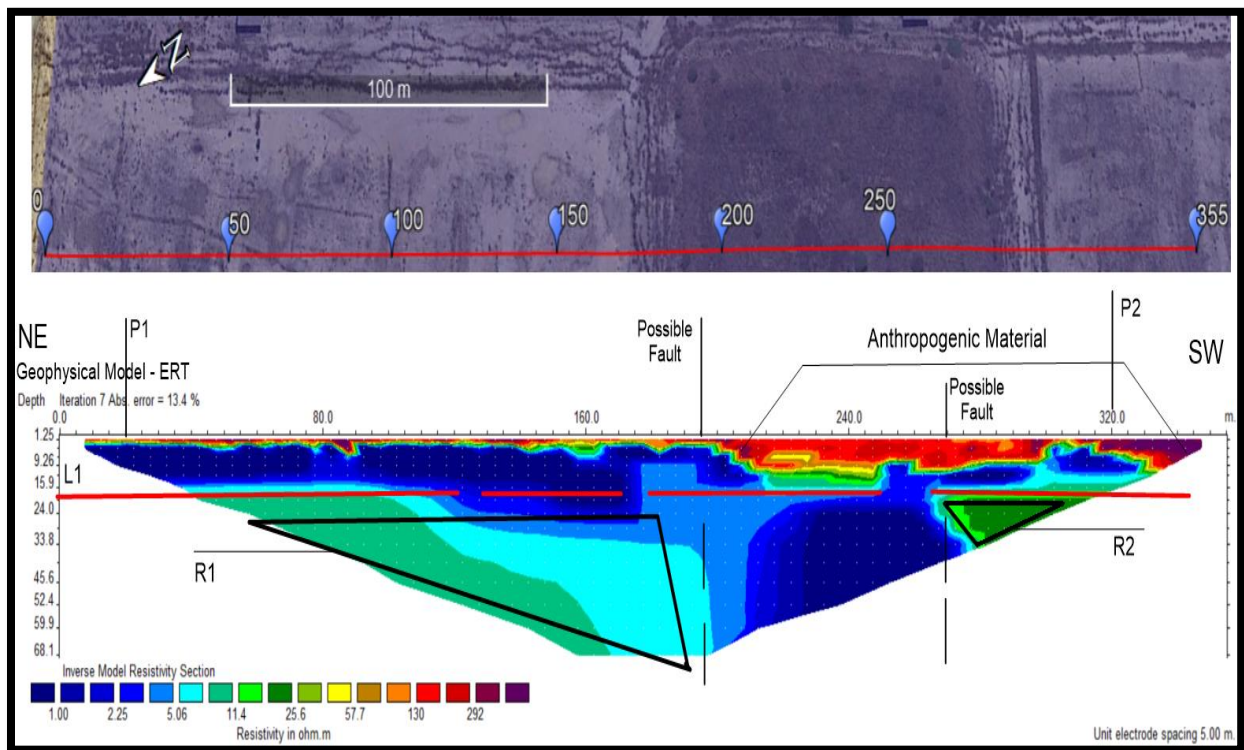


Figure 39. Results from Profile 3, ERT. Location of resistive bodies (R1-R2). Black vertical dashed lines – Possible faults. Black vertical lines – Interception with P1 and P2. Engineering and geotechnical purposes.

1.8. Conclusions.

The main objective of this research was to apply and compare electrical and electromagnetic methods in two cases: locating groundwater contamination, and characterizing the bedrock and subsidence detection for geotechnical purposes.

In the first case of study was possible to identify the contaminated zones as well as fault zones with water circulation in both profiles (P1 and P2).

- ◆ In ERT profiles, it was possible to obtain resistivity values that indicate the presence of contaminated groundwater. These zones are well confirmed (C1 and C2 in Fig. 35 and 36). It was also possible to identify the geological materials constituting the area, supported by the geological maps (Fig.2). It was also confirmed the existence of 8 faults, perpendicular to the profiles that influence the hydrodynamic of the area.
- ◆ The ERT was found to be an excellent method for identifying areas with high resistivity contrasts by easily identifying potential contamination risk zones. Moreover, the application of the electrical resistivity method allowed the characterization of a large area of study, quickly and inexpensively.
- ◆ The FDEM method detected better the main structures than the small ones and the results were quite positive mainly for P2. It was also detected variations of resistivity in agreement with the ERT in both profiles. Proving this to be a useful method in a pre-analysis in the subsurface observation of the crust, because it is fast acquisition (each reading takes about 30s), low cost and low acquisition logistics.

For geotechnical purposes, the results were also satisfactory. The applied techniques allowed to identify fractured zones of the bedrock, as well as zones with clay content, being zones of low mechanical robustness that are subject to subsidence when it is applied high compression.

- ◆ The ERT method confirms the existence of 3 layers, with resistivities of 50-200, 1 and 10-30 ohm.m, from top to the bottom, which were detected by TDEM and FDEM method, (Fig.37, 38 and 39). Their thickness is irregular along with the profile, however, it is clearly seen the 5 m thickness of the first layer which corresponds to the anthropogenic material. The low resistivity values (1-5 ohm.m) in the second layer confirm the presence of clays, considered as subsidence risk zone.
- ◆ Due to the irregularity of the layers in the ERT method, the location of the bedrock is uncertain. However, the results of TDEM and FDEM methods are very satisfactory and indicate the depth of the bedrock at 25-30 m.

- ◆ The FDEM method shows a very agreement with TDEM and ERT profiles in a quantitative response and it identifies the three layers with accuracy.

The ability to characterize sub-surface structures makes the ERT, TDEM, and FDEM methods a powerful tool for both localization of contaminated waters and analysis of subsidence and bedrock zones.

As a timeless risk, groundwater contamination should be monitored regularly, preventing from releasing contaminants into the environment, leading to public health risk. While for geotechnical proposes, geophysical methods are cost-effective to characterize large areas when compared with conventional ground investigation methods like boreholes, CPT, DMT among others, as well as the capacity of reaching deeper depths with good resolution

These methods, together with laboratory analyzes and other types of direct methods, play a fundamental role in better understanding and interpreting the physic properties of the material and with that, be able to identify possible risk zones.

2. APPARENT CONDUCTIVITY CALCULATION AND OPTIMIZATION IN FDEM-8.

2.1. Introduction.

The measurement data that are obtained from geophysical instruments (FDEM) are not intuitively related to the subsurface resistivity/conductivity and layer thickness. The measurements obtained by electromagnetic instruments can be expressed in voltage (V), mutual impedance (Z), real and quadrature components of the amplitude or amplitude (A) and phase ($^{\circ}$). This makes it difficult to compare measured quantities in different places, especially if the parameters of the measure (frequency, time and magnitude of transmitter current) are different, (Butler, 2005). The apparent resistivity is a parameter that helps to compare different measurements with different measurement parameters.

Apparent resistivity, introduced by Wenner (1912) and Schlumberger (1920), is a useful concept for interpretation of the data, in general, better than raw data. For electrical methods, the apparent resistivity can be calculated using the observed field as it was saw in section 1.3. However, for EM it's not possible to solve explicitly for the half-space the apparent conductivity values in terms of the observed field, (Van der Kruk *et al.*, 2000).

Therefore, several apparent conductivities definitions for frequency domain soundings, have been formalized and used over the years. One of them uses an asymptote for the field of a magnetic dipole in a homogeneous half-space and is useful only for low induction number (McNeill 1980), which result in a linear relationship between the measured quantity and conductivity of the subsurface. Another definition introduced by Wilt and Stark (1982) uses only the amplitude of the total magnetic field, although it's a non-unique result.

In the case of FDEM-8, the measurements are express as amplitude and phase of the secondary magnetic field in the receptor. In the present work, the apparent resistivity was calculated using the LIN formula but the inphase component of Z is calculated using a full solution of the induction phenomena. Further, a non-linear inversion of the data was performed, using a 1-D inversion with a 2-D smoothness constraint between adjacent 1-D models, which lead to a final rough representation of a 2D model. The forward and inversion algorithm was produced and described in Monteiro Santos, (2010).

2.2. Apparent Conductivity Definition.

The apparent conductivity does not represent the real conductivity of the ground. It is defined as the conductivity of a homogeneous half-space which will produce the same response as that measured over the real earth with the same acquisition parameters (position, transmitted current), (Spies and. Eggers, 1986).

In electromagnetic methods, this relation between apparent conductivity and the real conductivity is complex because they don't depend linearly on each other. However, in certain conditions, is possible to find a linear relationship between those parameters.

2.3. Apparent Conductivity (σ_a) in optimization.

In the present work, the FDEM-8 data was used to investigate the subsurface. The data was acquired in a horizontal coplanar configuration (HCP), generating a vertical magnetic dipole source (VMD). When the transmitter and the receiver are located on the surface of a homogeneous half-space the solution of the magnetic field ratio (McNeill, 1980) is expressed by:

$$\frac{H_s}{H_p} = \frac{2}{\gamma^2 r^2} [-9 + (9 + 9i\gamma r - 4\gamma^2 r^2 + \gamma^3 r^3) e^{-\gamma r}] \quad (2.3.1)$$

Where H_s is the secondary magnetic field at the receiver, H_p is the primary magnetic field in the free-space and γ is a complex function of frequency and conductivity, called wave number. However, for certain conditions, this equation can be simplified. Taking into account the concept of skin depth mentioned previously (section 1.3.2, eq. 1.3.14), therefore:

$$\gamma r = \sqrt{2i} \frac{r}{\delta} \quad (2.3.2)$$

Where $\frac{r}{\delta}$ is the called induction number, B :

$$\gamma r = 2iB \quad (2.3.3)$$

In the case of a low induction number, which means $\gamma r < 1$ the fields' ratios of the eq. 2.3.1 can be reduced to a simpler expression:

$$\frac{H_s}{H_p} = 1 + \frac{iB^2}{2} = 1 + \frac{i\omega\mu_0\sigma r^2}{4} \quad (2.3.4)$$

This means, that the in-phase (or real part) component of the ratio is unit and does not depend on the conductivity, while the quadrature (or imaginary part) does. Therefore, when the frequencies of the electromagnetic field are very low, which correspond to low values of the induction number B , the imaginary (or quadrature) part of the magnetic field is directly proportional to conductivity, while the actual (in-phase) part is independent of these parameters (McNeill 1980):

$$\sigma_a = \frac{4}{w\mu_0 r^2} \text{imag}\left(\frac{H_s}{H_p}\right) \quad (2.3.5)$$

Therefore, a linear relationship between the imaginary part of the magnetic field and the conductivity of the ground is established which leads, for a heterogeneous and layered half-space, to a cumulative response, (Butler, 2005):

$$\frac{H_{zs}}{H_{zp}} = 1 + \frac{iw\mu_0\sigma r^2}{4} \sum_{m=1}^N \sigma_m Q_m^G \quad (2.3.6)$$

Where, Q_m^G is the geometric factor which gives the cumulative response of the various layers as a function of the normalized depth, σ_m is the conductivity of the m^{th} layer until a maximum of N layers.

Equation (2.3.5) has been used in the calculation of apparent conductivity for instruments operating at a low induction number and eq. (2.3.6) was later used in 1-D laterally constrained inversion, for forward and derivatives calculations, [Monteiro Santos, (2004); Monteiro Santos *et al.*, (2009)].

However, in highly conductive environments, the apparent conductivity it's known to be non-linear (Monteiro Santos *et al.*, 2010), which led to the optimization of a more robust inversion algorithm. Therefore, a full expression of the magnetic field for the apparent conductivity calculation in a layered earth was used, instead of the cumulative function formulation that is usually used for low frequencies.

For a homogeneous half-space, the apparent conductivity can be solved using equation 2.3.1. However, for a layered half-space is more complex, and the half-space has to be divided into horizontal layers. Therefore, following Keller and Frischknecht (1966) and Monteiro Santos (2010), for a vertical dipole (HCP) source, the secondary components over an N-layered model is given by:

$$H_{zs} = -\frac{m}{4\pi\delta^3} T_0(A, B) \quad (2.3.7)$$

Where m is the magnetic moment of the source, and T_0 is defined as:

$$T_0 = \int_0^{\infty} R_0\left(\frac{gB}{r}\right) g^2 e^{-2gA} J_0(gB) dg. \quad (2.3.8)$$

In this equation, g is the variable of integration, J_0 is the Bessel function of the first kind of order 0, $gB/r = \lambda$ and $A = \frac{h}{\delta}$, in the present case, the h value is 0, however for a stable solution a very close number to 0 is given. For a layered model $R_0(\lambda)$ is defined by the following recursion relationship:

$$R_0(\lambda) = \frac{k_0 + Z_1}{k_0 + Z_1} \quad (2.3.9)$$

Where k_0 is a complex function of frequency and conductivity, and it's given by:

$$k_i = \frac{\sqrt{\lambda^2 + j\sigma_i\mu_i w}}{j\mu_i w} \quad (2.3.10)$$

With $j = \sqrt{-1}$, i represents the i^{th} layer where $i=N$ is the deepest, and Z is given by:

$$Z_i = k_i \frac{Z_{i+1} + k_i \tanh(u_i t_i)}{k_i + Z_{i+1} \tanh(u_i t_i)} \quad (2.3.11)$$

Where t_i is the thickness of the i^{th} layer and goes from 1 to N-1. For a vertical dipole source, the primary component over an N-layered model is given by:

$$H_{zp} = \frac{m}{4\pi} \left[\frac{3(z-h)^2}{R^5} - \frac{1}{R^3} \right] \quad (2.3.12)$$

Setting $z=h=0$, for a dipole source located on the ground, the previous equation can be simplified as:

$$H_{zp} = \frac{m}{4\pi} \frac{1}{R^3} \quad (2.3.13)$$

Therefore, the solution of the magnetic field ratio with $B = \frac{R}{\delta}$ and recalling the equation 2.3.7 is given by:

$$\frac{H_{zs}}{H_{zp}} = B^3 \int_0^{\infty} R_0(gB/r) g^2 e^{-2gA} J_0(gB) dg. \quad (2.3.14)$$

The predicted values of the quadrature component for HCP configuration placed on the ground is:

$$Q_{HCP} = \text{Im}\left(\frac{H_{zs}}{H_{zp}}\right) \quad (2.3.15)$$

So, equations (2.3.14), (2.3.15) and (2.3.5) were used in this work.

2.4. Non-Linear Inversion of FDEM Data.

The objective of geophysical inversion is to find a model that gives a response that fits to the measured values. The model is an idealized mathematical representation of a section of the earth, which has a set of model parameters that are the physical quantities we want to estimate from the observed data. The model response is the synthetic data that can be calculated from the mathematical relationships defining the model for a given set of model parameters. All inversion methods essentially try to determine a model for the subsurface whose response agrees with the measured data subject to certain restrictions (Loke, 2012).

In the present work, a nonlinear smoothness-constrained least square method was used. This method has been used for decades to invert EM data in 1D soundings. The application of this method in 2 D case, however, creates an unstable solution. For minimizing this problem a smoothness-constrain was applied, which finds the smoothest change for which the residual error is contained within the desired tolerance, (Sasaki, 1989).

This method represents a 1-D laterally constraint approach, which leads to a final rough representation of a 2D model based on a large number of blocks, with a constant resistivity. Its distribution and size depend on the locations and the intercoil spacing, (Monteiro Santos, 2004).

Inversion programs, due to their non-linear relationship, usually use iterative methods that require partial derivatives of the model response with respect to the model parameters. Here, the logarithms of the earth conductivity σ and of the measured quadrature amplitude (Q_a^o) are used as the model parameter and data set, respectively.

After the forward model response calculation through a full expression of the magnetic field, the equation for optimization (Monteiro Santos, 2010) is:

$$(W_d J^T W_d J + \lambda C^T C) \delta \vec{p} = W_d J^T W_d \delta \vec{d} \quad (2.4.1)$$

Where W_d is the accuracy of the measured data with the reciprocal of the data variances, J is the Jacobian matrix, which contains the partial derivatives of the model response in respect to the model parameters, and is defined as:

$$J_{ij} = \frac{\sigma_j}{Q_{a,i}^c} \frac{\partial Q_{a,i}^c}{\partial \sigma_j} \quad (2.4.2)$$

Where σ_j is the calculated, apparent conductivity for the j^{th} block. The λ is called the Lagrange parameter (damping factor), which controls the amplitude of the parameter correction and it is empirically determinate, for the present case, in the beginning of the iteration process, $\delta \vec{p}$ is a vector which contains the corrections to the model parameters, $\delta \vec{d}$ is the vector of the difference between the logarithms of the model response (Q_a^c) and the measured data (Q_a^o), C is a matrix whose values are the coefficients of the

roughness in each parameter. This roughness has the contribution of the neighbor's blocks and can be express, (Monteiro Santos, 2004):

$$\delta r_j = \delta p_{jE} + \delta p_{jW} - 4\delta p_j + \delta p_{jN} + \delta p_{jS} \quad (2.4.3)$$

Where, E, W, N, and S are the four immediate neighbors of the j^{th} block.

From the initial model, the programs seek to improve the model until the misfit between the observed and the calculated data is reduce to a minimal error, (Monteiro Santos, 2010).

2.5. Results.

The results of 1-D laterally constrain inversion were quite satisfactory considering the data quality. The profile results are shown in Figures 40, 41 and 42 for P1, P2, and P3 respectively, and described below. For all models, the initial uniform resistivity was 100 ohm.m.

For P1, Fig. 40 shows the results of three inversion processes where 7 of the 8 possible frequencies were used (2400, 1200, 600, 300, 150, 75 and 37 Hz), with the largest being withdrawn (4800 Hz) due to their low 'force', representing anomalous values in relation to the others. Data were obtained with a transmitter-receiver spacing of 10 m.

- ◆ In the first process (A), the convergence was achieved up to 8 iterations and no longer converging thereafter, with a damping factor (λ) of 0.3. As stated earlier, the damping factor (Lagrange parameter) is a controller of the parameter correction amplitude, so a less smooth result was found for this process, with the misfit ranging from 20-30%, which is due mainly to the quality of the data.
- ◆ For the second process (B), the results obtained are smoother than the previous one, resulting from the damping factor used ($\lambda = 3$). This model was obtained after 19 iterations, and no longer converging after that. There was a misfit in the order of the previous one, with values between 20-30%.
- ◆ For the third process (C), the results obtained are the smoothest of all processes ($\lambda = 30$), and the iteration process that best fit the ERT data (Fig.35) in terms of resistivity values. The registered misfit has the same order as the previous ones, 20-30%. This process was obtained after 31 iterations and ceased to converge after that. It's worth mentioning that the lower values for the damping factor does not result in a better fit between the model responses to the data.

For P2, Fig. 41 shows the result of two inversion processes where 7 of the 8 possible frequencies were used (2400, 1200, 600, 300, 150, 75 and 37). Not to mention the non-convergence of the data to a damping factor

of 0.3, therefore for this value, there are no results. The data were obtained with a transmitter-receiver spacing of 20 m.

- ◆ In the first process (A), convergence was achieved up to 23 iterations, no longer converging thereafter. In this process, a damping factor of 3 was used, which made the result less smooth compared to the subsequent result. For this process, the resulting misfit was slightly lower than P1, with values between 15-25%, which indicates a better fit to the data in this profile.
- ◆ In the second process (B), the damping factor used was 30 leading to an apparent smooth model. However, it is not as visible as in P1, possibly because it is not so stratified. The model converged to 34 iterations, then failed to converge after that. The percentage of misfit for this process was similar to that of the first, 15-25%. This was the model chosen and that best fit the ERT, Fig.36.

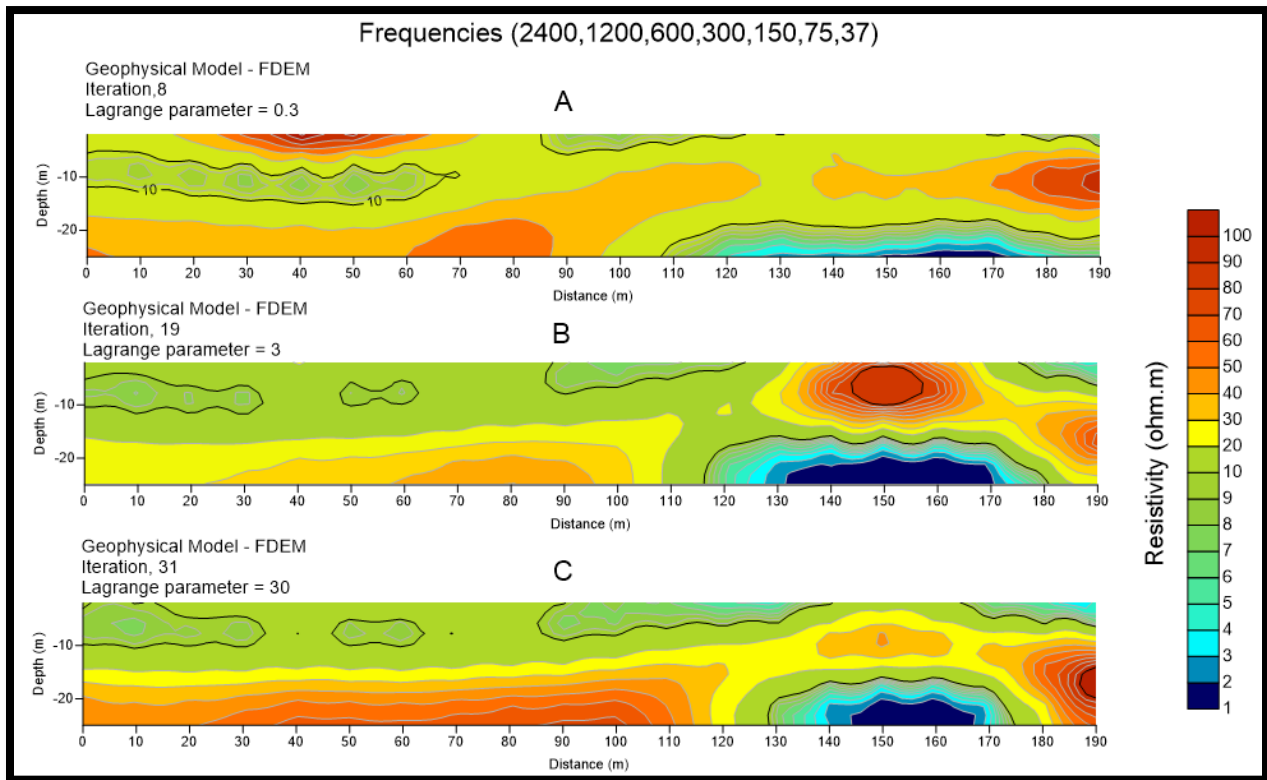


Figure 40. FDEM inversion from a nonlinear smoothness-constrained least square method; A - for 8 iterations and a Lagrange parameter = 0.3; B - for 19 iterations and a Lagrange parameter = 3; C - for 31 iterations and a Lagrange parameter = 30.

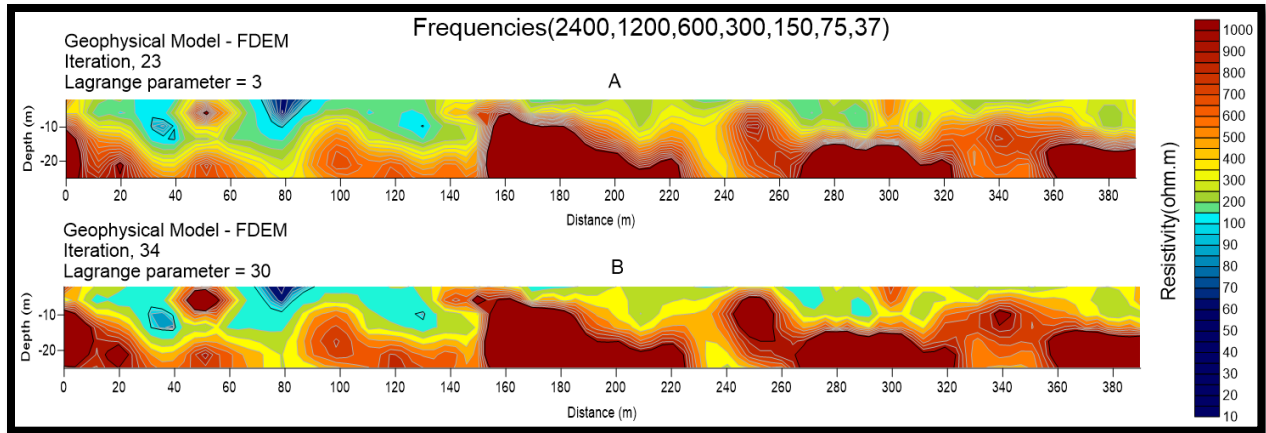


Figure 41. FDEM inversion from a nonlinear smoothness-constrained least square method; A - for 23 iterations and a Lagrange parameter =3; B – for 34 iterations and a Lagrange parameter = 30.

For P3, Fig. 42 shows two inversion processes (A and B). As in P2, for a damping factor of 0.3, convergence was not achieved. The frequencies used were the same as the previous profiles, and the transmitter-receiver spacing was 20 m. In relation to the previous profiles, the geology of this site is different, presenting a higher stratification.

- ◆ In the first process (A) a damping factor of 3 was used, leading to convergence up to 22 iterations and no longer converging thereafter. It presents resistivity values similar to the ERT, however, it presents a very high misfit $\pm 50\%$. Terrain conditions and data noise can explain much of the high misfit value.
- ◆ In the second process (B), the damping factor was increased to 30 and the model converged to 31 iterations, ceasing to converge thereafter. This was the model used in comparison with the TDEM and ERT profiles (Fig.37) since it presented a slightly lower misfit than process A and as a result of the damping factor value used, presented a smoother model compatible with the stratified medium.

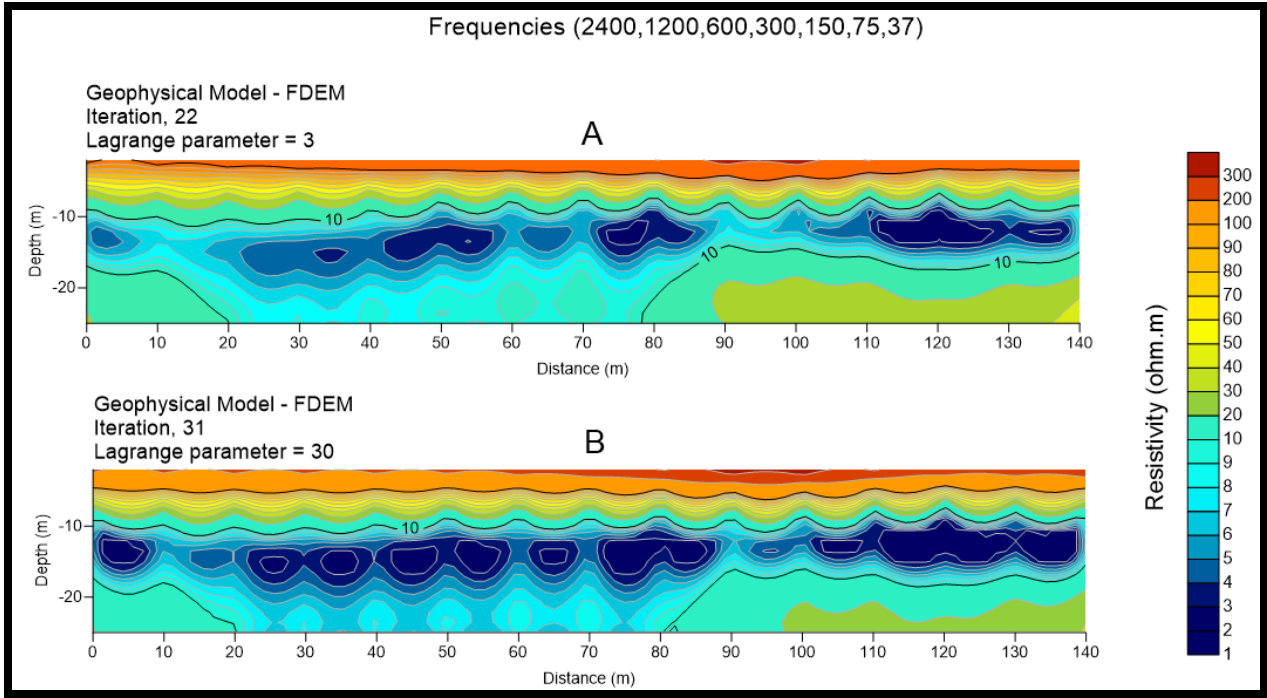


Figure 42. FDEM inversion from a nonlinear smoothness-constrained least square method; A - for 22 iterations and a Lagrange parameter =3; B – for 31 iterations and a Lagrange parameter = 30.

2.6. Conclusions.

The data of the FDEM-8 equipment, which works with frequencies between 4800 Hz and 37 Hz, has been used in the last decade as a qualitative method. Here, the apparent conductivity was used in an inversion process using a nonlinear least square method with a smoothness-constrain in order to get a quantitative data interpretation.

The main conclusion of this work is that, for this frequency electromagnetic equipment (FDEM-8), the forward model calculation, from a full expression of the magnetic field, produced very good results. Therefore, a 1-D laterally constrained inverse method to quantify the results acquired from FDEM-8 was successfully done.

The high misfit values, in relation to the data, for a transmitter-receiver spacing of 20 m is mainly due to the data quality, which is influenced by several factors: accuracy of the distance between transmitter and receiver, loops orientation and level, electromagnetic noise.

The results obtained are in agreement with those obtained by ERT and TDEM methods. A damping factor (λ) value of 30 was chosen in all the FDEM profiles for this comparison, mainly because it has slightly lower misfit values than the other λ values.

Despite satisfactory results, for a good interpretation of the geophysical properties, better quality control of the data must be done. It's clearly seen in P3 the high values of resistivity in the first layer will create noise in the higher frequencies (2400 Hz), because of their low energy, which influences the results in the inversion process. This could be one of the reasons for the high value of the misfit presented in this profile. Therefore, a very high control of the initial measured data must be done, not only for these frequencies but also for the remaining.

The great advantage of this equipment is its transportability and speed of data acquisition. If we add a quantitative data interpretation, FDEM-8 becomes a very interesting tool for a pre-analysis of the physical properties of the soil, thereby identifying potential zones of interest.

3. References

- Abdul Nassir, S. S., Loke, M. H., Lee C. Y., (2001). Salt-water intrusion mapping by geoelectrical imaging surveys. *Geophysical Prospecting*, vol 48, Issue 4.
- Barus, C., (1882). The electrical activity of ore-bodies. U.S. Geological Survey. Bull., •884.
- Benson, A. K., (1995). Applications of ground-penetrating radar in assessing some geological hazards: examples of groundwater contamination, faults, cavities. *Journal of Applied Geophysics*, vol. 33, pp 177-193.
- Borner, F., Gruhne, M., and Schon, J. (1993). Contamination indications derived from electrical properties in the low frequency. *Geophysical Prospecting*, 41(1), 83–98.
- Butler, K. D., (Ed.), (2005). *Near-Surface Geophysics (Investigation in Geophysics No 13)*. Society of Exploration Geophysics, pp 732.
- Daniels, J. J., Keller, V. G., Jacobson, J. J., (1975). Computer-assisted interpretation of electromagnetic soundings over a permafrost section. *Society of Exploration Geophysicists*, vol 41, Issue 4, pp 592-797.
- Fox, R. W. (1830). On the Electro-Magnetic Properties of Metalliferous Veins in the Mines of Cornwall. *Philosophical Transactions of the Royal Society of London*, 120(0), 399–414.
- Gonçalves, R., Farzamian, M., Monteiro Santos, F. A., Represas, P., Mota Gomes, A., Lobo de Pina, A. F., Almeida, E. P., (2017). Application of Time-Domain Electromagnetic Method in Investigating Saltwater Intrusion of Santiago Island (Cape Verde). *Pure and Applied Geophysics*, vol 174, Issue 11, pp 4171-4182.
- Griffiths, D.H., and Barker R. D., (1993). Two-dimensional resistivity imaging and modeling in areas of complex geology. *Journal of Applied Geophysics*, vol 29, Issue 3-4, pp 211-226.
- Heen, Z., Muhsen, S., (2016). Application of Vertical Electrical Sounding for Delineation of Sea Water Intrusion into the Freshwater Aquifer of Southern Governorates of Gaza Strip, Palestine. *IUG Journal of Natural Studies* vol 24, No 2.
- Kaufman, A.A., Keller, G.V. (1983). Frequency and transient soundings. *Methods in Geochemistry and Geophysics* No 16. Elsevier, N.Y.
- Keller, G. V. (1988). *Rock and Mineral Properties. Electromagnetic Methods in Applied Geophysics*.
- Keller, G. V., Frischknecht, F. C., (1966). *Electrical methods in geophysical prospecting*. Pergamon Press Inc., Oxford.
- Loke, M. H. (2011). *Electrical Resistivity Surveys and data Interpretation*. Geotomo Software Sdn. Bhd., Gelugor, Penang, Malaysia.

- Loke, M. H. (2012). Tutorial: 2-D and 3-D electrical imaging surveys. Geotomo Software Sdn. Bhd., Gelugor, Penang, Malaysia.
- Lopes, I., Tavares, G., Ferreira, G., Peniche, B., and Santos, J., (2018). Joint Inversion of MASW and Rayleigh Wave Ellipticity in the Site Characterization of PLLN Alluvial Area, VFX, N Lisbon. 24th European Meeting of Environmental and Engineering Geophysics.
- McNeill, J. D. (1980). Electromagnetic terrain conductivity measurement at low induction numbers. Geonics Limited, Technical Note TN-6.
- McNeill, J. D. (1990). Use of Electromagnetic Methods for Groundwater Studies. Geotechnical and Environmental Geophysics, vol. 1, Review and Tutorial.
- Monteiro Santos, F. A., (2004). 1-D laterally constrained inversion of EM34 profiling data. *Journal of Applied Geophysics*, vol 56, Issue 2, pp. 123-134.
- Monteiro Santos, F. A., (2006). Capítulo 4: Técnicas para investigação de estruturas superficiais – Métodos indutivos. *Prospecção Geofísica*. Faculdade de Ciências da Universidade de Lisboa (FCUL).
- Monteiro Santos, F.A., Mateus, A., Figueiras, J., Gonçalves, M.A. (2006). Mapping groundwater contamination around a landfill facility using the VLF-EM method – a case study. *Journal of Applied Geophysics* 60, 115–125.
- Monteiro Santos, F.A., Triantafyllis, J., Taylor, R., Holladay, S., Bruzgulis, K.E., (2010). Inversion of conductivity profiles from EM using full solution and a 1-D laterally constrained algorithm. *Journal of Engineering and Environmental Geophysics* 15, 163–174.
- Mota, R., Monteiro Santos, F. A., Mateus, A., Marques, F.O., Gonçalves, M.A., Figueiras, J., Amaral, H., (2004). Granite fracturing and incipient pollution beneath a recent landfill facility as detected by geoelectrical surveys. *Journal of Applied Geophysics*, vol 57, Issue 1, pp. 11-22.
- Nabighian, M. N. (Ed.), (1988). *Electromagnetic Methods in Applied Geophysics*, pp 991.
- Oliveira, J. T., Pereira, Z., Carvalho, P., Pacheco, N., Korn, D., (2004). Stratigraphy of the tectonically imbricated lithological succession of the Neves Corvo mine area, Iberian Pyrite Belt, Portugal. *Mineralium Deposita*, vol 39, Issue 4, pp 422–436.
- Orange, A. S., (1989). Magnetotelluric exploration for hydrocarbons. *Institute of electricians and Electronics Engineers*, vol 77, Issue 2, pp. 287–317.
- Park, S. K., & Dickey, S. K. (1989). Accurate Estimation of Conductivity of Water from Geoelectrical Measurements- A New Way to Correct for Clay. *Ground Water*, 27(6), 786–792.
- Sasaki, Y., (1989). Two-dimensional joint inversion of magnetotelluric and dipole-dipole resistivity data. *Geophysics* 54, pp 254– 262.

- Sharma and Baranwal (2005). Delineation of groundwater-bearing fracture zones in a hard rock area integrating very low frequency electromagnetic and resistivity data. *Journal of Applied Geophysics*, vol 57, Issue 2, pp. 155-166.
- Schlumberger, C., 1920. Study of underground electrical prospecting. Paris, 99 pp.
- Spies, B. R., Eggers, D. E., (1986). The use and misuse of apparent resistivity in electromagnetic methods. *Society of Exploration Geophysics*, vol 57, Issue 7.
- TEM-FAST 48 HCP manual, (2007), version 7.3. Applied Electromagnetic Research (AEMR), the Netherlands.
- TEM-Researcher manual, (2007), version 7. Applied electromagnetic Research (AEMR), the Netherlands.
- Triantafilis, J., Monteiro Santos, F. A., (2010). Resolving the spatial distribution of the true electrical conductivity with depth using EM38 and EM31 signal data and a laterally constrained inversion model. *Australian Journal of Soil Research* 48(5) 434-446.
- Van der Kruk, J., Meeke, J. A. C., Van den Berg, P. M., Fokkema, J. T., (2000). An apparent-resistivity concept for low-frequency electromagnetic sounding techniques. *Journal of Geophysical Prospecting*, vol 48, No 6, pp. 1033-1052.
- Wait, J. R., (1951). The Magnetic Dipole over the Horizontally Stratified Earth. *Canadian Journal of Physics*, 29(6), 577–592.
- Wait, J. R. (1955). Mutual Electromagnetic of Loops over a Homogeneous Ground. *Geophysics*, 20(3), 630–637.
- Ward, S. H., (1990). Resistivity and Induced Polarization Methods. *Geotechnical and Environmental Geophysics*, vol. 1, Review and Tutorial.
- Wenner, F. (1912). Characteristics and Applications of Vibration Galvanometers. *Transactions of the American Institute of Electrical Engineers*, XXXI (1), 1243–1254.
- Zbyszewski, G., Torre de Assunção, C., (1965) – Geological Chart of Portugal in 1/50 000 scale and Explanatory News Sheet 30-D Alenquer. Geological Services of Portugal.